Medium term hydrochemical and CO2 responses to anthropogenic and environmental changes in karst headwater streams

F. Ulloa-Cedamanos, J.L. Probst, Anne Probst

Science of the Total Environment 957 (2024) 177614

Contents lists available at ScienceDirect

Science of the Total Environment

journal homepage: www.elsevier.com/locate/scitotenv

Medium term hydrochemical and CO_2 responses to anthropogenic and environmental changes in karst headwater streams

F. Ulloa-Cedamanos [a,b,c,d,*], J.L. Probst [a,b,c], A. Probst [a,b,c,*]

[a] Centre de Recherche sur la Biodiversité et l'Environnement (CRBE), Université de Toulouse, CNRS, IRD, Toulouse INP, Université Toulouse 3 – Paul Sabatier (UT3), Toulouse, France
[b] LTER Bassin versant du Baget, SNO Karst, IR OZCAR, CNRS, University of Toulouse, France
[c] LTSER Zone Atelier Pyrenees-Garonne, CNRS, University of Toulouse, France
[d] Research Institute for Environment and Livelihoods, Charles Darwin University, Darwin, NT 0909, Australia

HIGHLIGHTS

- We analyzed hydrochemical data from 20 karst catchments over the past two decades.
- Seasonal changes are driven by hydrological conditions in karst headwaters.
- Rising CO_2 trends were linked to reforestation and agricultural changes in uplands.
- Rising cation concentration trends were linked to decreased discharge in lowlands.
- Natural and anthropogenic changes directly affect water chemistry in karst systems.

GRAPHICAL ABSTRACT

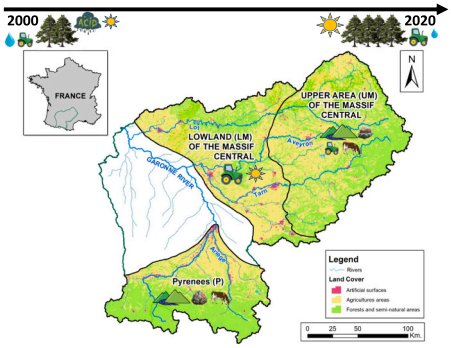

ARTICLE INFO

Editor: JV Cruz

Keywords:
Trends
Land use
pCO_2
Weathering
Regional
Acidity sources
Climate change

ABSTRACT

This study investigates the intricate effects of lithology, temperature, discharge, and land use changes on headwater stream chemistry by analysing two decades of hydrochemical data from twenty karst headwater catchments in the Garonne River basin, France. Focused on the Pyrenees and the lowland (LM) and upland (UM) regions of the Massif Central, this study identified significant regional variations and commonalities in water chemistry. The headwater streams were clustered based on their hydrological and hydrochemical profiles, revealing strong similarities between upland sites, i.e. UM and Pyrenees, despite their geographical distance. The findings revealed a predominance of water driven by calcite dissolution, with specific influences from minor lithologies. Seasonal variations in water chemistry were primarily driven by hydrological conditions. Trend analyses highlighted increased pCO_2 concentration in both the Pyrenees and UM, linked to higher forest density and agricultural activities, respectively. In contrast, LM exhibited increasing Ca^{2+} and HCO_3^- concentrations alongside decreasing trends in pCO_2 and discharge, and increased nitrate concentration. While overall water temperatures increase, only a few sites exhibited significant warming trends, consistent with similar studies in the region and worldwide. These findings underscore the complex interplay between land use changes and hydrochemical dynamics in karst headwaters. They reveal that rising pCO_2 concentration trends in upland

* Corresponding authors.
E-mail addresses: francesco.ulloacedamanos@cdu.edu.au (F. Ulloa-Cedamanos), anne.probst@toulouse-inp.fr (A. Probst).

https://doi.org/10.1016/j.scitotenv.2024.177614
Received 4 July 2024; Received in revised form 1 October 2024; Accepted 16 November 2024

regions are driven by reforestation and agricultural practices, which have significant implications in CO_2 emissions, and consequently for regional and global carbon budgets and carbon-related policies. In lowland areas, declining water resources and increasing ion concentrations highlight potential challenges for water management, particularly in sensitive karst catchments. This study provides a baseline for understanding how karst headwaters respond to environmental changes. Expanding this research to other karst systems worldwide, under different climates, would help validate and model these findings, and improve our understanding of the global carbon cycle.

1. Introduction

Carbon (C) is constantly cycled between the atmosphere, lithosphere, hydrosphere, and terrestrial pools. In terrestrial ecosystems, an estimated 6.40 ± 3.00 PgC yr^{-1} is fixed as organic matter (Regnier et al., 2022). The decomposition of this organic matter, together with autotrophic respiration, enriches soils with carbon (Li, 2019; Stockmann et al., 2013). This soil organic carbon can either leach vertically into groundwater, transfer laterally to surface waters, or remain stored in soils (Bauer et al., 2013; Cole et al., 2007).

Leached C enriches groundwater with carbon dioxide (CO_2), which is essential for the natural chemical weathering of crustal rocks (Amiotte Suchet et al., 2003). Chemical weathering is a key process in the global carbon cycle (Amiotte Suchet and Probst, 1995; Garrels and Mackenzie, 1971; Zeng et al., 2019). As silicate and carbonate rocks undergo weathering, they consume CO_2 and release dissolved inorganic carbon (DIC), primarily as bicarbonate (HCO_3^-), within waters with a pH range between 6.4 and 10.3 (Dreybrodt, 1988; Schulte et al., 2011). Silicate weathering serves as the only long-term net carbon sink, capable of sequestering carbon over timescales >0.1 million years. In contrast, carbonate dissolution acts as a sensitive short-term carbon sink, highly susceptible to anthropogenic drivers such as acid rain (Yuanrong et al., 2021), nitrogen fertilizers (Perrin et al., 2008), and land use change (Raymond et al., 2008; Zeng et al., 2021). Among environmental drivers, temperature plays a crucial role, with the optimal range for carbonate dissolution between 5 and 15 °C, typical of temperate climates (Gaillardet et al., 2019; Mujalli Romero, 2019). In colder environments, scarce vegetation limits CO_2 availability (Calmels et al., 2014; Romero-Mujalli et al., 2018), while warmer conditions may constrain CO_2 solubility and the vegetation productivity (Dreybrodt, 1988; Zeng et al., 2021). Increased runoff enhances carbonate dissolution by exposing more reactive mineral surfaces and renewing saturated waters with diluted one (e.g., rainwater) (Zeng et al., 2016). However, extreme and prolonged increases in runoff can dilute water by less concentrated water, and reduce interaction time between water and rock, lowering weathering rates (Ran et al., 2015; Ulloa-Cedamanos et al., 2021a). Soluble minerals, such as evaporites, can promote carbonate precipitation when total dissolved solids (TDS) concentrations exceed 6 meq L^{-1} (Meybeck, 2003). Other minerals, like pyrite, can produce strong acids, replacing carbonic with sulphuric acid as the primary source of acidity (Table S1). Recent studies have reported rising chemical weathering fluxes, both at the site-specific (Gislason et al., 2009; Macpherson and Sullivan, 2019; Raymond et al., 2008; Ulloa-Cedamanos et al., 2021b) and global scale (Xiong et al., 2022). However, mid- to long-term studies of stream C based on direct observations in headwater streams remain scarce due to the lack of temporal datasets (Liu et al., 2024).

Transferred C to fluvial waters is predominantly released back to the atmosphere, with an estimated 2.25 ± 0.90 PgC yr^{-1} emitted (Regnier et al., 2022). Though headwater streams cover only a small portion of the catchment surface, they act as hot spots for carbon emissions, playing a vital role in the global carbon budget (Marx et al., 2017; Wallin et al., 2018). Most of these emissions occurs within a few hundred meters downstream from groundwater sources (Johnson et al., 2008), and this distance can be even shorter in turbulent areas with steep topography (Rocher-Ros et al., 2019), typical of mountainous catchments. Yet, small watersheds are globally under-surveyed for all carbon species, particularly in upland regions (Liu et al., 2024). Temporal data are also limited in frequency and duration, particularly in headwater streams. Consequently, understanding the effects of environmental changes —such as land use or habitat alteration— has often relied on space-for-time substitutions rather than direct long-term observations (Stanley et al., 2023). While this approach has provided valuable insights into carbon and water quality seasonal dynamics (Zeng et al., 2021), our knowledge of these processes in headwater streams and their responses to past and current disturbances, remains limited.

Headwater streams in karst terrains frequently originate from springs where groundwater re-emerges at the surface. Karst systems are geomorphological structures formed through combined processes of chemical weathering and mechanical erosion acting on soluble rock, particularly carbonates, which covers 13 to 15 % of the world's ice-free land (Amiotte Suchet et al., 2003). Of these karst formations, 69 % are located in mountainous regions worldwide (Chen et al., 2017; Goldscheider et al., 2020). Understanding the hydrochemical dynamics of karst systems is crucial given their significant role in the global carbon cycle (Liu et al., 2018), their sensitivity to climate change (Szczypta et al., 2015; Zeng et al., 2019), their role as reservoirs —storing 25 % of the world's drinking water— (Ford and Williams, 2007), and their contribution to the dissolved ion export, accounting for 45 to 60 % of the total DIC transported to the oceans (Amiotte Suchet et al., 2003; Gaillardet et al., 1999). In karst systems, land use directly influences soil respiration (Gwiazda and Broecker, 1994) and affects the sources of acidity that contribute to rock weathering (Zeng et al., 2017, 2021, 2019). In forested areas, carbonic acid derived from organic matter oxidation is the primary source of acidity, whereas in anthropized areas, other acids compete for dominance in weathering processes (Gandois et al., 2014; Perrin et al., 2008; Probst et al., 1995). Human activities, such as agriculture and fossil fuel combustion, significantly impact rock weathering and consequently influence water quality. Residues from these activities can rapidly reach karst groundwater, contaminating watercourses (Yue et al., 2019). Likewise, the decline of these activities can trigger changes in water quality. Forest restoration on formerly agricultural land can lead to significant shifts in primary production, contributing to increased soil organic matter content (Coxon, 2011) and stock (Wiśniewski and Märker, 2021), and enhanced soil respiration (Sheng et al., 2010). Land use change, coupled with global warming, could affect the quality and discharge of headwater streams (Ulloa-Cedamanos et al., 2022; Zeng et al., 2021). Additionally, acid rain—containing sulphuric acid from fossil fuel combustion—has historically been another anthropogenic source of acidity. However, in Western Europe, this source has decreased since the early 21st century (Pascaud et al., 2016a, 2016b) due to stricter environmental regulations (Coddeville et al., 2016).

In France, about one-third of the land surface is underlain by carbonates susceptible to karstification. In southwest France, karst systems are predominantly found within the Garonne basin, which is categorized as an active to hotspot region for chemical weathering (Lechuga-Crespo et al., 2020). Like many karstic regions worldwide, the spatial dynamics and trends of headwater chemistry —across varying lithologies, hydroclimatic conditions, and land use changes— remain poorly understood (Binet et al., 2020; Ulloa-Cedamanos et al., 2022). To address these knowledge gaps, the present study focuses on twenty headwater karst catchments in the upper Garonne basin over an eighteen-year

period. The research aims to (i) establish a hydrological and hydrochemical baseline for the region, (ii) identify medium-term trends in water quality at the selected sites, and (iii) determine the causal relationships between observed environmental changes and trends in headwater stream chemistry. The primary hypothesis is that the selected environmental parameters—such as lithology, discharge, temperature, and land use changes—drive spatial and temporal changes in water chemistry in these headwater karst systems. However, temporal changes in these parameters are expected to vary across regions, leading to distinct trends in water chemistry within these sensitive Karst Critical Zones (K-CZ).

2. Materials and methods

2.1. Study area

The Garonne River basin, a major French river basin, covers an area of 52,000 Km^2 at the Mas d'Agenais hydrological station (Fig. 1A, Etchanchu and Probst, 1988; Probst and Bazerbachi, 1986). Probst and Tardy (1985) identified three regions with distinct geological structures and hydroclimatic conditions: the Aquitaine sedimentary basin surrounded by the Massif Central to the northwest (Fig. 1B) and the Pyrenees to the south (Fig. 1C) (Etchanchu and Probst, 1988; Probst, 1983), reaching maximum altitudes of 1900 and 3000 m, respectively (Amiotte Suchet and Probst, 1996). Since this research focuses on the primary karstic sources within the Garonne basin, the Pyrenees and Massif Central regions were selected for detailed study (Fig. 1).

The Massif Central, located on a high plateau, influences a vast plain region. Made up of Jurassic limestones, the Massif Central underwent tectonic movements in the Tertiary period, resulting in faults and harbouring karstic aquifers (Brunet and Coppolani, 1970). In addition to limestone, volcanic rocks from the Tertiary and Quaternary periods also cover the Massif Central (Semhi et al., 2000). The hydrological regime is pluvio-oceanic, characterized by both oceanic and Mediterranean conditions, resulting in lower summer rainfall and drying winds (Kessler and Chambraud, 1990; Probst and Tardy, 1985). Annual precipitation in the Massif Central, ranging from 900 to 1050 mm (Roy and Négrel, 2001), exceeds that in the lowlands (Meersmans et al., 2012) due to the influences of humid Atlantic and Mediterranean air masses on the foothills of the Massif Central. Although the highest peak in the Massif Central (1885 m) is not comparable to that in the Pyrenees (3404 m), its hydrological contribution to the total Garonne River discharge represents 62 % (Probst and Tardy, 1985). The predominant soils in this region are Cambisols, Luvisols, and some less developed soils such as Leptosols and Andosols. The land cover in the Massif Central is dominated by forests and pastures, closely followed by heterogeneous agriculture. By contrast, the lowland region is mainly covered by agricultural lands and pastures (Fig. 1B).

The Pyrenean part of the Garonne basin covers about one-third of the Pyrenean Mountain range (Grusson, 2016; Probst and Bazerbachi, 1986). The Pyrenees can be broadly classified into three large units: (i) the central axial zone with terrains of gneisses, Precambrian granites, and schists, (ii) the northern Pyrenean zone comprising pre-Jurassic metamorphic terrains, and (iii) the southern Pyrenean zone, dominated by terrains composed of limestones, marlstones, and Mesozoic schist (Probst and Bazerbachi, 1986; Semhi et al., 2000). The hydrological regime is transitional nival type, characterized by high flows in spring and low flows in summer, sometimes extending into autumn (Probst and Bazerbachi, 1986). Over a period of 65 years, the average interannual discharge at the outlet of the Pyrenean area of the Garonne basin stands at 217 $m^3 s^{-1}$ upstream from Toulouse, with annual rainfall ranging from 600 to 1000 mm and peaks reaching up to 3600 mm, with a decreasing gradient from west to east (Fig. 1C, Probst and Bazerbachi, 1986). The predominant soils are Cambisols, with some karstic areas with less developed soils. Upstream, the land cover is dominated by forests and alpine meadows. As the terrain descends into the lowlands, the landscape changes abruptly to heterogeneous agricultural areas associated with pastoralism and, eventually, irrigated agriculture (Fig. 1C).

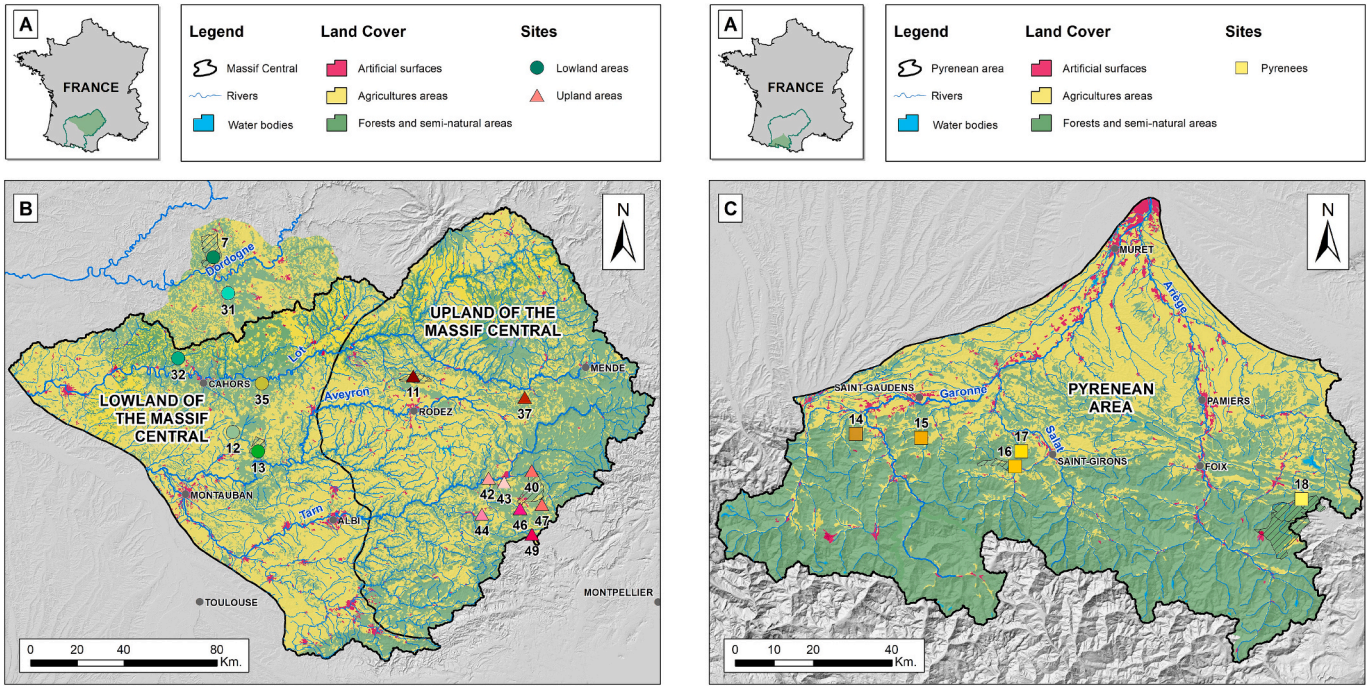

Fig. 1. (A) Geographical location of the study areas in the Garonne River basin (outlined in green) and in France. Hill shade, hydrographic network, and land cover of (B) the Massif Central and (C) the Pyrenees. Sites, along with the ID number (see Table 1), are marked with reddish triangles, greenish circles, and a yellowish square for the upland and lowland of the Massif Central and the Pyrenean region, respectively. Two additional sites in the Dordogne basin, a downstream tributary of the Garonne basin, are also included. Catchment areas are delineated only for sites 7, 11, 13, 16, 18, and 40, included in the temporal analysis.

2.2. Selection of target sites

The selection of sampling sites began by identifying over one hundred karst catchments within the Pyrenees and the Massif Central regions of the Garonne basin. However, given the scarcity of complete hydrological (Eau France, 2024), physico-chemical and chemical data (ADES database, 2024), only sites with more than two samples per year since the 2000s were chosen for the spatial approach of this mid-term study. The labels of these sites remained unchanged after applying the filtering criteria. This selection resulted in twenty sites draining karst terrains spread over three regions located in the upstream areas of the Garonne basin (Fig. 1).

To extend the applicability of the results to adjacent karst catchments and improve the robustness of the dataset, two additional sites (sites 7 and 31) located in the nearby Dordogne River basin, a downstream tributary of the Garonne River, were included (Fig. 1A).

Interannual trends in headwater streams were studied at representative sites with a large number of samples in both the Massif Central and the Pyrenees. In the Massif Central, sites 7, 13 (LM), 11 and 40 (UM) were selected, while in the Pyrenees, sites 16 and 18 were chosen. Although site 16, known as Baget catchment, did not show any significant trends (Table S3) due to the limited number of water samples of this dataset (Table 1), previous studies have confirmed its representativeness for the typical evolution of an undisturbed karst catchment in the Pyrenean region (Mangin, 1975; Sivelle et al., 2019; Ulloa-Cedamanos et al., 2021a), including trends in water chemistry (Ulloa-Cedamanos et al., 2020). Additionally, site 18 exhibited trends contrasting with the other sites, and was therefore studied as an exceptional case in the Pyrenees.

2.3. Hydrochemical survey

The hydrological (Eau France, 2024), physico-chemical and chemical data (ADES database, 2024) for the twenty sites selected in the upper reaches of the Garonne River basin covered the period from approximately 2000 to 2018, with an average of 18 years of monitoring per site. The sites located at lower altitudes are in the lowland of the Massif Central (LM), with a mean elevation of 144 ± 25 m, which contrasts with the sites in the upland of the Massif Central (UM, 504 ± 115 m) and the Pyrenees (487 ± 36 m). As most of the sites are in low-lying mountainous areas (UM and Pyrenees), the mean and median elevations are notably high, at 392 and 446 m, respectively (Table 1). Water discharge measurements were taken hourly, other parameters were measured 2 to 3 times per year at most sites. Exceptions include sites 7, 31, 32, and 35, which were monitored monthly (Table 1).

The liability of the chemical analysis of major ions concentrations was evaluated using ionic balance calculations, expressed as (ΣCation – ΣAnion)/(ΣCation + ΣAnion)*200, in equivalent (eq), based on the principle of solutions electroneutrality. Over 80 % of the samples had ionic balances lower than 5 % (1478 measurements), and 99.5 % of the samples had ion balances lower than 10 %.

2.4. Alkalinity loss

Alkalinity loss (ΔAlk, Eq. 1), expressed as an equivalent percentage, quantifies the production of $Ca^{2+} + Mg^{2+}$ from carbonate and silicate weathering by various pathways (Table S1). In calcareous substrates, strong acids, such as the sulphuric and nitric acid, are rapidly neutralized by carbonate dissolution (Nicholson et al., 1988). Therefore, the deviation from the theoretical line 1:1 between HCO_3^- and $(Ca^{2+}+Mg^{2+})$, quantified by ΔAlk, can be attributed to silicate and carbonate weathering by strong acids, as well as evaporate dissolution.

$$\Delta_{Alk}(\%) = \frac{\left(Ca^{2+} + Mg^{2+}\right) - HCO_3^-}{\left(Ca^{2+} + Mg^{2+}\right)} \times 100 \quad (1)$$

2.5. Statistical analysis

All statistical methods were performed using R software. The analysis incorporated major dissolved elements and environmental parameters, including water discharge, specific discharge, water temperature, and pCO_2 in water (Table 1).

Hierarchical clustering analysis (HCA) is a widely used multivariate statistical technique that groups a large number of objects (in this study, sampling sites) into smaller groups with similar profiles (in this study, water chemistry and environmental features). It works by creating a hierarchy of clusters that can be represented in a tree-like diagram called a dendrogram (Cloutier et al., 2008). The number of clusters was determined by the linkage distance threshold. In this study, the threshold was set at 5 to delimit three clusters (C1 to C3) based on the environmental characteristics, and the chemical composition of the headwater streams.

Principal Component Analysis (PCA) positions the study variables along two axes, capturing their relative variations through underlying factors, also known as principal components (Laffitte, 1972). These factors are linear combinations of the original variables, constructed to maximize the variance explained in the dataset. Factor loadings reveal the strength of the correlation between each variable and the principal components, with positive values indicating a strong positive correlation and negative values indicating a strong negative correlation (Kaiser, 1958).

Redundancy analysis (RDA) is a two-stage multivariate technique that begins with linear regression of individual and environmental data, resulting in a matrix of fitted values. These fitted values are then used in PCA to generate canonical axes, which are linear combinations of the predictors (Legendre and Legendre, 2012). This approach allows for the simultaneous analysis of multiple individual characteristics and environmental predictors (Forester et al., 2018; Sytiuk et al., 2020). The significance of each explanatory variable in the RDA was assessed using 1000 permutations to determine the *p*-values.

PCA and RDA are sensitive to the scale of the variables. Standardization of the data, such as transforming variables to have zero mean and unit variance, is necessary to ensure that variables with different units or scales do not disproportionately influence the results. To address this, we standardized the raw data using log-ratio transformation with the "clr" function in the *compositions* package and the "decostand" function in the *vegan* package. Although these methods do not require the data to be perfectly normally distributed, the analysis performs better when the data approximates a normal distribution. We used the Shapiro-Wilk test to assess normality, which yielded p-values below 0.05. High intercorrelation between parameters and multicollinearity among predictors can impact the stability and interpretability of PCA and RDA results. To address this limitation, we selected the least autocorrelated variables that were also the most representative of the hydrochemical processes in the catchment. For instance, pH was excluded due to its high correlation with pCO_2, while TDS and conductivity were omitted because of their significant correlations with Ca^{2+} and HCO_3^-.

Linear and Reduced Major Axis (RMA) fit methods were used as linear regression models. These two methods aim to minimize the sum of squares of the residuals using the vertical or perpendicular distance between each data point and the regression line, respectively. Of all the linear fit trends (Table S2), only those with a significance level (p-value) < 0.2 were considered (Table S3), given the limited number of significant trends observed in the regions studied. This choice was influenced by the low number of observations per year, which was a constraint on statistical analyses despite the medium-term monitoring period (Table 1).

Table 1
Average values of hydrochemical and physico-chemical parameters in headwater streams for the selected sites in the Pyrenees (P) and Massif Central (Lowland-LM and Upland-UM). The parameters are Y (number of monitoring years), H (elevation of the basin outlet), Q (annual mean of discharge), Qs (specific discharge), N (number of samples), Tw (water temperature), pCO_2 (partial pressure of CO_2, log pCO_2), Cond (specific conductivity), TDS (total dissolved solids), and major cations and anions (from Ca^{2+} to NO_3^-).

Sites	Y	H	Q	Qs	N	Tw	pH	pCO_2	Cond	TDS*	Ca^{2+}	Mg^{2+}	Na^+	K^+	HCO_3^-	SO_4^{2-}	Cl^-	NO_3^-
	count	meters	L s^{-1}	L Km^{-2} s^{-1}	count	°C	–	atm	µS cm^{-1}	mg L^{-1}	µmol L^{-1}							
P-14	15	530	406	22.6	30	10.3	7.8	-2.6	303	260	1332	286	52	8	3025	89	60	43
P-15	15	460	93	34.3	30	12.5	7.8	-2.5	392	343	1895	252	71	8	4065	59	72	38
P-16	15	496	490	37.0	30	10.2	7.7	-2.5	327	276	1530	190	46	12	3078	174	44	43
P-17	15	441	441	37.1	30	10.0	7.9	-2.6	346	304	1550	369	49	8	3666	37	45	47
P-18	26	510	1804	21.2	42	9.5	7.5	-2.2	326	284	1559	225	50	11	3259	110	54	45
Mean P	**17**	**487 ± 36**	**647**	**30 ± 8**	**32**	**10.5 ± 1.2**	**7.7**	**-2.5**	**339 ± 33**	**293 ± 32**	**1573 ± 203**	**264 ± 68**	**54 ± 10**	**9 ± 2**	**3419 ± 440**	**94 ± 53**	**55 ± 12**	**43 ± 3**
LM-7	18	123	646	7.3	203	13.6	7.2	-1.7	535	469	2722	148	149	34	5364	59	190	185
LM-12	22	170	399	5.7	44	14.2	7.0	-1.4	645	590	3448	179	153	26	6897	66	206	140
LM-13	20	165	265	5.0	41	13.8	7.0	-1.4	668	601	3418	296	182	43	6813	87	260	291
LM-31	25	108	147	7.1**	196	13.2	7.1	-1.6	584	513	3006	159	164	31	5750	173	198	154
LM-32	25	138	122	6.8	224	13.4	7.1	-1.6	618	545	3137	190	189	41	6255	65	245	201
LM-35	18	160	387	10.5	214	13.5	7.1	-1.5	639	565	3299	139	205	36	6505	71	241	173
Mean LM	**21**	**144 ± 25**	**328**	**7 ± 2**	**154**	**13.6 ± 0.3**	**7.1**	**-1.5**	**615 ± 48**	**547 ± 50**	**3172 ± 277**	**185 ± 58**	**174 ± 22**	**35 ± 6**	**6264 ± 606**	**87 ± 43**	**223 ± 29**	**191 ± 54**
UM-11	15	450	482	13.8	38	12.1	7.5	-1.9	613	536	2636	736	122	50	6087	97	169	333
UM-37	26	720	15	13.2**	41	10.1	7.6	-2.1	513	450	2207	624	124	17	5282	67	180	125
UM-40	18	400	1040	10.5	61	11.8	7.4	-2.0	448	382	1845	586	113	14	4422	64	140	160
UM-42	18	340	65	13.2**	32	13.2	7.5	-1.9	535	453	1546	1392	125	39	5235	112	178	266
UM-43	23	500	272	13.0	40	11.8	7.5	-2.0	435	368	1856	473	112	13	4147	72	153	226
UM-44	19	420	82	13.2**	40	12.3	7.6	-2.1	638	543	2306	1281	117	28	5376	712	168	209
UM-46	18	595	189	11.1	33	11.0	7.6	-2.2	421	354	1489	776	94	13	4202	50	122	124
UM-47	23	533	1579	14.6	47	11.3	7.5	-2.1	434	368	1574	792	119	9	4295	47	164	159
UM-49	18	578	1045	16.1	32	10.5	7.6	-2.2	412	348	1365	851	129	14	4190	40	127	83
Mean UM	**20**	**504 ± 115**	**530**	**13 ± 2**	**40**	**11.6 ± 1.0**	**7.5**	**-2.0**	**494 ± 85**	**422 ± 77**	**1869 ± 431**	**835 ± 309**	**117 ± 10**	**22 ± 14**	**4804 ± 704**	**140 ± 216**	**156 ± 22**	**187 ± 79**

(*) TDS = $Ca^{2+} + Mg^{2+} + Na^+ + K^+ + HCO_3^- + SO_4^{2-} + Cl^- + NO_3^-$, protons and ammonium being neglectable.
(**) Specific discharge represents the regional average for the respective sites.

3. Results

3.1. Hydrochemical characteristics

The main characteristics of each site are summarized in Table 1, with all sites grouped according to their geographical distribution (Fig. 1). The outlet elevation of the catchments ranges from 108 to 720 m. Specific water discharge shows marked spatial variation between the Massif Central as a whole and the Pyrenean region. Water temperature values are higher and relatively stable in the LM compared with the UM and the Pyrenees. Conversely, pH values show an inverse trend, with more alkaline waters in the UM and the Pyrenees. The partial pressures of CO_2 (pCO_2) calculated in the LM waters are very close to the soil pCO_2, unlike the UM and the Pyrenees. Total dissolved solids (TDS) and specific conductivity followed a similar spatial distribution to pCO_2, with the highest values observed in the LM (Table 1).

Among the main dissolved elements, calcium (Ca^{2+}) predominated as the major cation (Table 1), representing between 51 % and 93 % of the total sum of cations in meq L^{-1} (Fig. 2). This wide variation can be attributed to the presence of magnesium (Mg^{2+}), whose percentages varied from 4 % to 46 % of the cation sum (Fig. 2). As a result, the Ca^{2+}/Mg^{2+} ratio (meq/meq) showed significant differences ($p < 0.01$) among these three regions, with the LM showing the highest ratio (18 ± 4), followed by the Pyrenees (6 ± 2), and the UM (3 ± 1). Concerning the anions, bicarbonate (HCO_3^-) emerged as the main anion (Table 1), displaying a narrower range of variation than Ca^{2+}, between 75 % and 96 % of the anion sum. Fluctuations in the relative contribution of HCO_3^- were offset by variations in the contribution of sulphate (SO_4^{2-}), ranging from 2 % to 20 %, and nitrate ions (NO_3^-), ranging from 1 % to 5 %. Sites with high SO_4^{2-} concentration were observed at sites 16 (Pyrenees), 31 (LM) and 44 (UM) (Fig. 2). If we consider the median values for each region, the contribution of HCO_3^- to the anion sum remains constant at 91 % across all areas, while the contribution of SO_4^{2-} is higher in Pyrenees (5 %) than in the Massif Central (2 %). This pattern is reversed for NO_3^-, with a higher contribution in the Massif Central (3 %) than in the Pyrenees (1 %) (Fig. 2).

3.2. Site clustering

The groups identified in the HCA (Fig. 3A) correspond to distinct geographical areas: C1 represents the lowland of the Massif Central (LM), C2 corresponds to the Pyrenees, and C3 pertains to the upland of the Massif Central (UM). The statistical distribution here indicated a greater similarity between the low-lying mountain sites, the UM and Pyrenees, compared to the LM, despite their relatively small geographic distances.

The distribution of sites on the PCA plot (Fig. 3B) confirmed the classification into three clusters representing each geographical area (Fig. 1), as shown in the HCA plot (Fig. 3A).

The first two PCA axes explained 64.6 % of the variance in the data. The first axis pitted water temperature (14 %) on the upper positive side of the plot, with pCO_2 (17 %), Cl^- (18 %), Na^+ (13 %), and NO_3^- (12 %) positioned on the lower negative side. This first axis contrasts the sites in the Pyrenees with those in the LM, with opposite values for these parameters (Table 1). The LM recorded the highest water temperatures and concentration of Cl^-, Na^+, NO_3^- and pCO_2, unlike in the Pyrenees. The second axis contrasted Ca^{2+} (34 %), HCO_3^- (32 %) and water temperature (10 %) in the positive axis, with NO_3^- (9 %), positioned in the negative axis. Dominated by Ca^{2+} and HCO_3^-concentrations, this axis partially grouped the UM (Ca^{2+} = 1.9 mol L^{-1}) and the Pyrenees (Ca^{2+} = 1.6 mol L^{-1}), contrasting them with the LM (Ca^{2+} = 3.2 mol L^{-1}). In addition, discharge, Mg^{2+}, and SO_4^{2-} were closely clustered, indicating

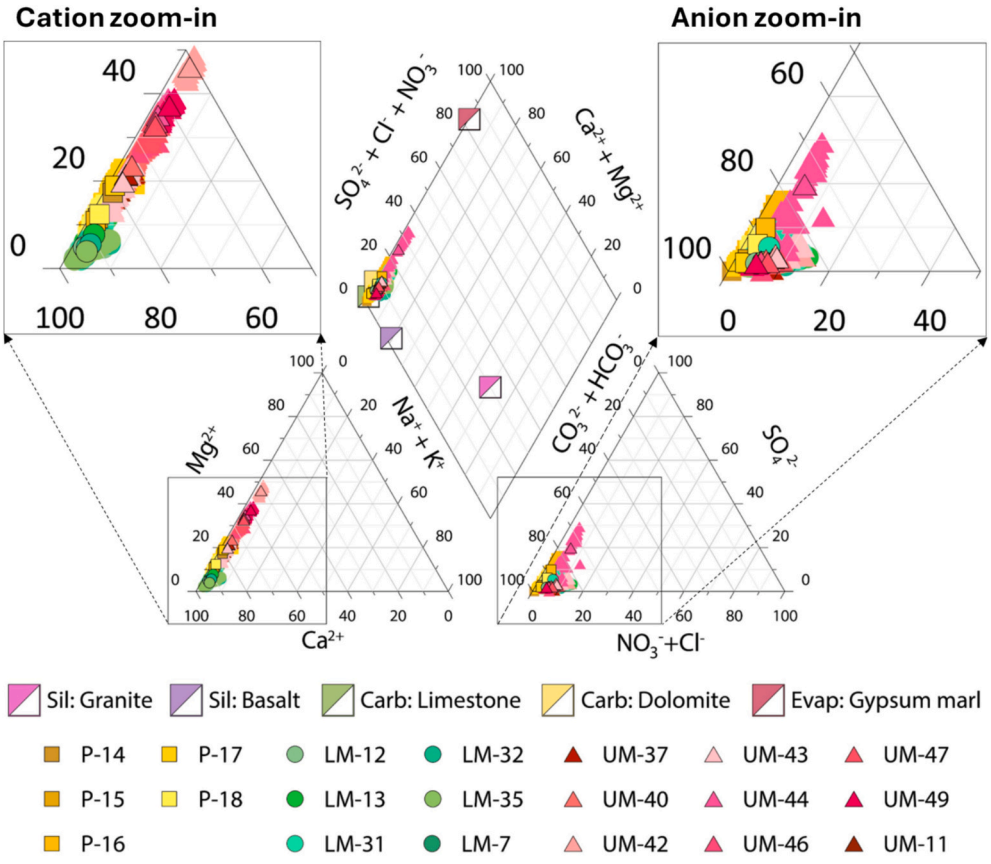

Fig. 2. Ternary Piper diagram showing cations and anions in the headwater streams of the twenty selected sites. The end-members values for the single rock types (adjusted for atmospheric inputs) in France are from Meybeck (2003).

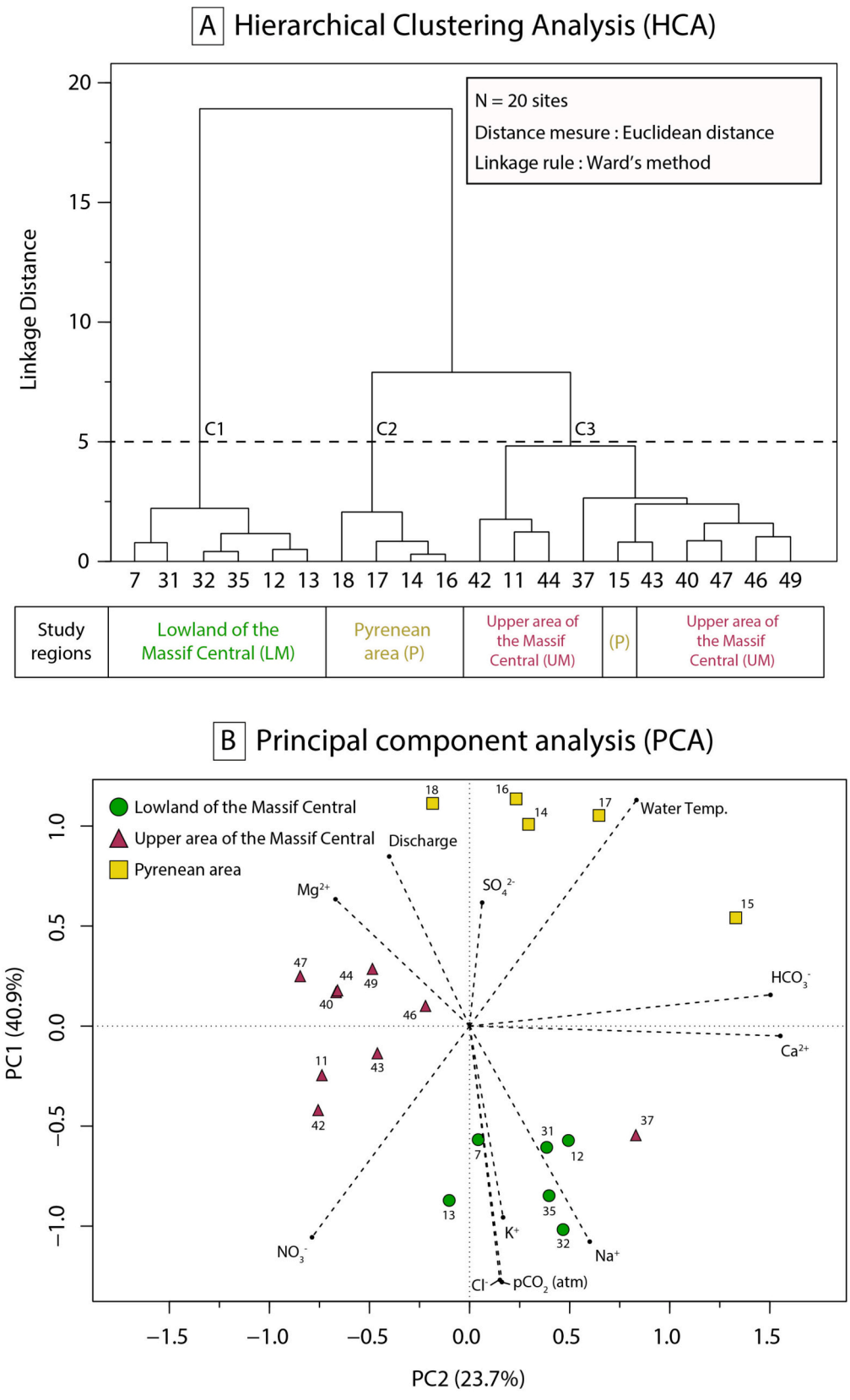

Fig. 3. (A) HCA and (B) PCA of the major element chemical composition (mmol L^{-1}), pCO_2 (atm), discharge (m^3 s^{-1}) and water temperature (°C) of the headwater streams at twenty selected sites.

similar variability, particularly among sites in the UM and Pyrenees.

3.3. Hydrochemical patterns

The headwater stream in the selected sites flows over carbonate-rich karst formations (Fig. 2). The most abundant carbonate mineral is the calcite ($CaCO_3$) in the Massif Central and the Pyrenees (Mangin, 1975). However, measured concentrations of (Ca^{2+}+Mg^{2+}) and HCO_3^- exceed those expected from the dissolution of pure calcite for a given pCO_2 (black dotted lines, Fig. 4A). Sites in the Pyrenees (indicated by yellowish squares) cluster closest to the carbonate dissolution pole, while the catchments in the Massif Central (LM, shown by greenish circles, and UM, by reddish triangles) display a minor influence from silicate hydrolysis and/or evaporite dissolution (Fig. 4B). This biplot reveals a shallower slope for the UM compared to the LM and Pyrenean region, indicating a higher HCO_3^-/Na^+ molar ratio for the same Ca^{2+}/

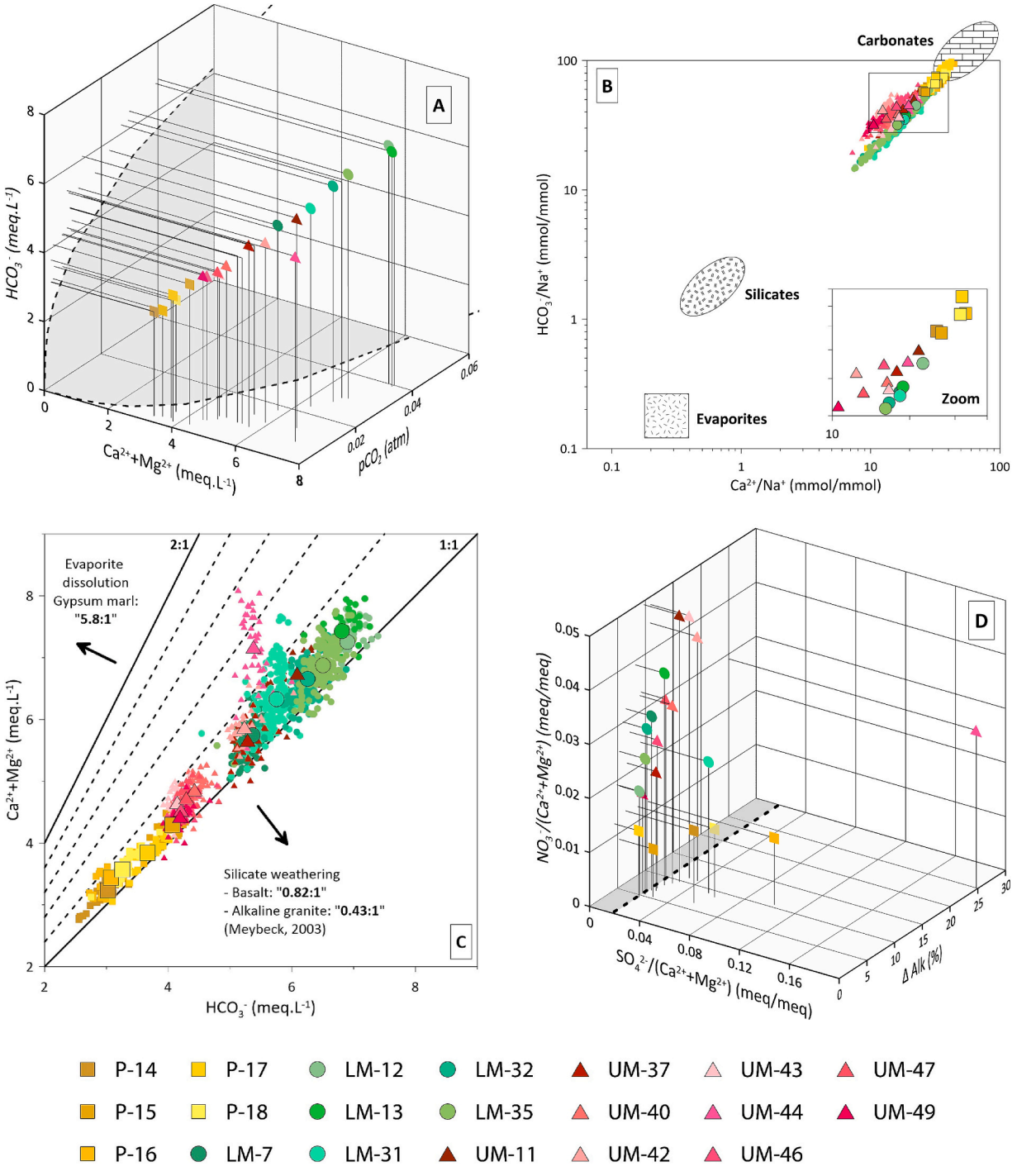

Fig. 4. (A) Carbonate dissolution as indicated by the concentrations of Ca^{2+}+Mg^{2+} and HCO_3^- (meq L^{-1}) as a function of pCO_2 (atm), with dashed black lines representing thermodynamic equilibrium with calcite at 10 °C, (B) Influence of lithological sources (carbonates, silicates and evaporites) on HCO_3^-/Na^+ plotted against Ca^{2+}/Na^+, (C) Relationship between (Ca^{2+}+Mg^{2+}) and HCO_3^-. The theoretical 1:1 and 2:1 lines indicate to the expected equivalent ratio (Ca^{2+} + Mg^{2+})/HCO_3^- for carbonates dissolution by carbonic acid and strong acids, respectively. The dashed lines have a difference in slope of 0.2 between them. (D) Relationship between average alkalinity loss (Δ Alk) and average ratios of $NO_3^-/(Ca^{2+}$ + $Mg^{2+})$ and $SO_4^{2-}/(Ca^{2+}$ + $Mg^{2+})$. The shaded area represents sulphates of atmospheric origin.

Na^{2+} molar ratio, suggesting another potential source of HCO_3^- in the UM region.

The sum of (Ca^{2+} + Mg^{2+}) accounted for 98 % of the total cations, while (HCO_3^- + SO_4^{2-} + NO_3^-) made up 97 % of the total anions (Fig. 2), resulting in an equivalent ratio (Ca^{2+} + Mg^{2+})/(HCO_3^- + SO_4^{2-} + NO_3^-) close to 1. A significant positive relationship was observed between (Ca^{2+} + Mg^{2+}) and HCO_3^- in headwater streams (Fig. 4C). However, nearly all the values were positioned above the theoretical 1:1 line for carbonate dissolution by carbonic acid, with many approaching the 2:1 line (Fig. 4C), particularly for site 44.

A wide disparity in the SO_4^{2-}/(Ca^{2+} + Mg^{2+}) ratio was highlighted in sites 16 and 44. Despite this, a common source of sulphate across the

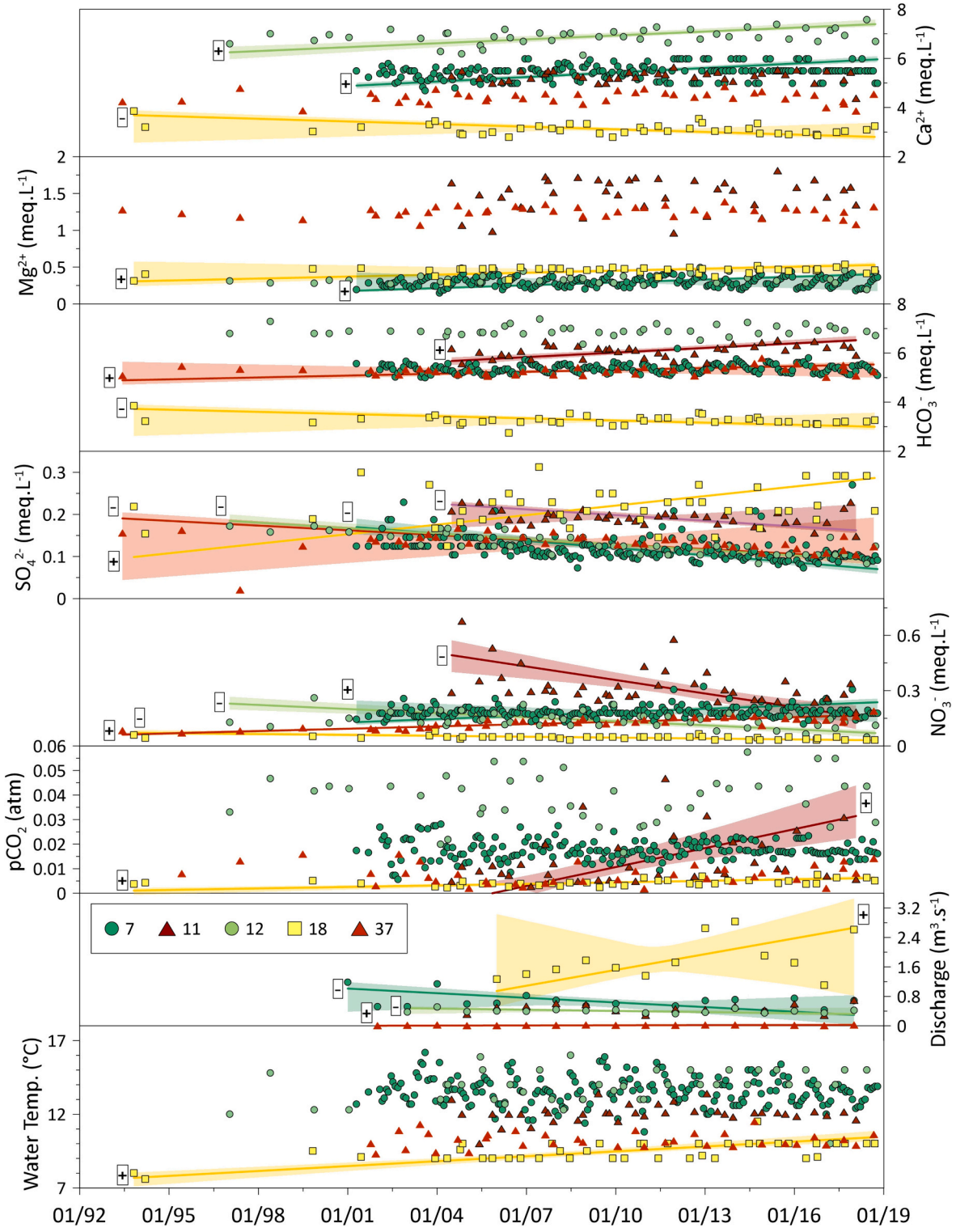

Fig. 5. Temporal trends of the instantaneous values of Ca^{2+}, Mg^{2+}, HCO_3^-, SO_4^{2-} and NO_3^- concentrations (meq L^{-1}), pCO_2 (1×10^{-2} atm), annual discharge (m^3 s^{-1}) and water temperature (°C) over the last two decades. The lines and shaded areas represent the RMA regression lines and 95 % confidence interval of the trends with $p >$ 0.2, respectively. Details of the RMA regressions are given in Table S4.

study sites was identified (shaded area below the dotted black line, Fig. 4D), which corresponds to the minimum and median value (0.02) of this ratio calculated for the twenty selected karst catchments. The ratio $NO_3^-/(Ca^{2+} + Mg^{2+})$ ratio remained consistently low and uniform in the Pyrenees (0.012, Fig. 4D). Conversely, this ratio displayed significant variability within the Massif Central, ranging from 0.015 to 0.050, with sites 13 (LM) and 11, 42, and 43 (UM) exhibiting ratios above 0.035.

3.4. Mid-term trends

Significant trends ($p < 0.2$) in dissolved elements, such as Ca^{2+} and Mg^{2+}, indicated an increase in the LM, while HCO_3^- trends increased in the UM (Table S3). In contrast to the previous trends observed at site 16 (Ulloa-Cedamanos et al., 2020), site 18 showed decreasing trends in Ca^{2+} and HCO_3^- concentrations in the Pyrenees. SO_4^{2-} concentrations decreased significantly at almost all sites studied, except for site 18.

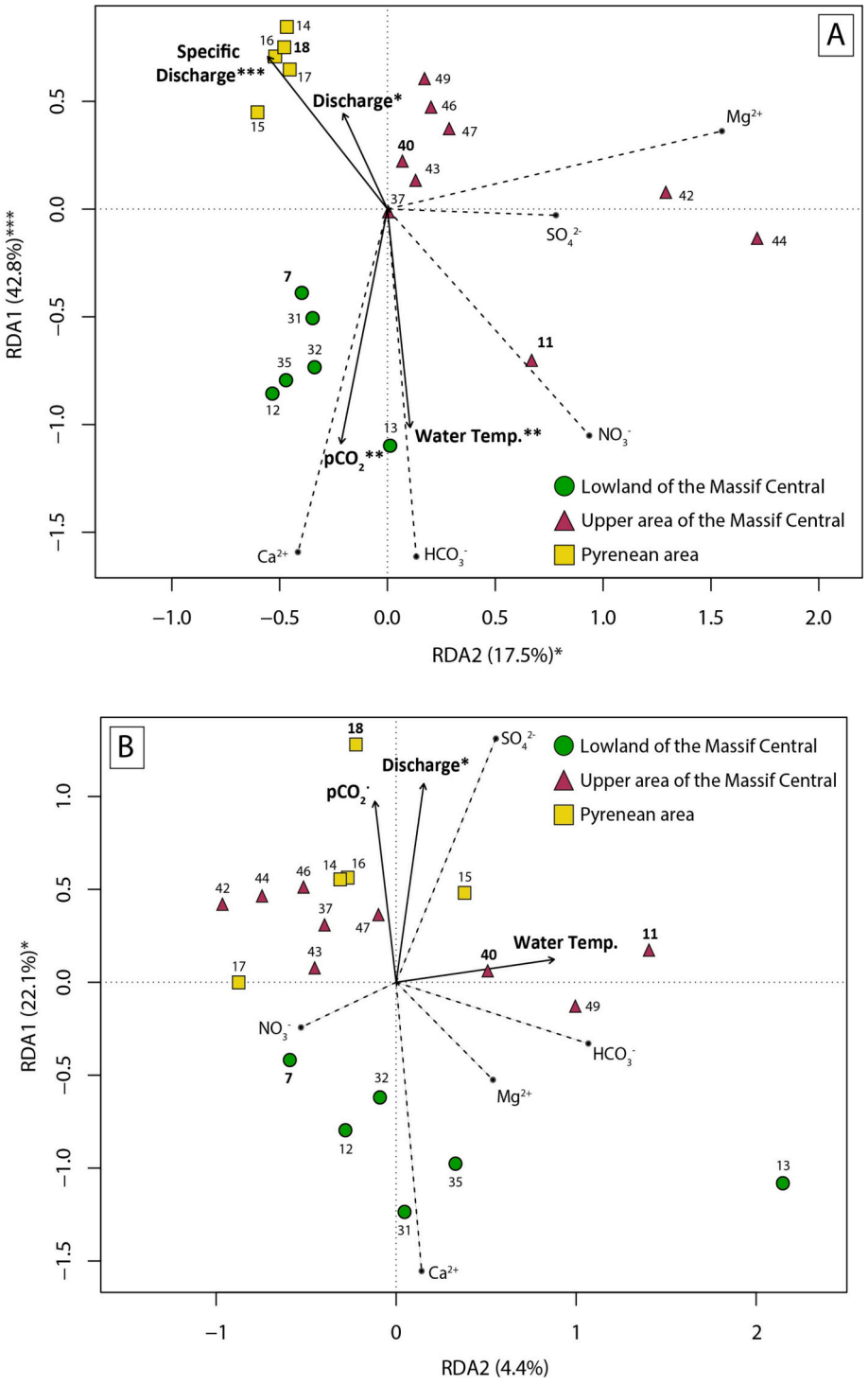

Fig. 6. (A) Redundancy analysis (RDA) of the average instantaneous values of headwater streams chemical composition (mmol L^{-1}) as a function of pCO_2 (atm), discharge (m^3 s^{-1}), specific discharge (L Km^2 s^{-1}), and water temperature (°C) for the twenty sites studied. (B) RDA of linear regression trends (p > 0.2) of water chemistry as a function of pCO_2, discharge and water temperature for the twenty study sites. Code meanings: "***" ($p \leq 0{,}001$), "**" ($p \leq 0.01$), "*" ($p \leq 0.05$) and "." ($p \leq 0.1$).

Unlike the Pyrenean sites, nitrates showed increasing trends in the UM, with the exception of site 11, where a decreasing trend was observed (Fig. 5).

Medium-term trends in environmental parameters revealed an increase in discharge and pCO_2 at the Pyrenean sites (site 18) and the UM sites (site 37), in contrast to the LM sites where discharge decreased. Positive trends in water temperature were observed across sites, but many were not significant, except in five catchments (Table S3), including site 18 (Fig. 5).

3.5. RDA in patterns and trends

The influence of environmental parameters—temperature, discharge, specific discharge, and pCO_2—on water chemistry was assessed using RDA, which explained 60.3 % of the variance (p-value <0.05) (Fig. 6A). The environmental parameters (lowest p-value <0.05) clustered into two groups (Fig. 6A). The first cluster is associated with high discharge (Q) in the Pyrenees and UM, and high specific discharge (Qs) predominantly in the Pyrenees, although Qs in the UM is still twice

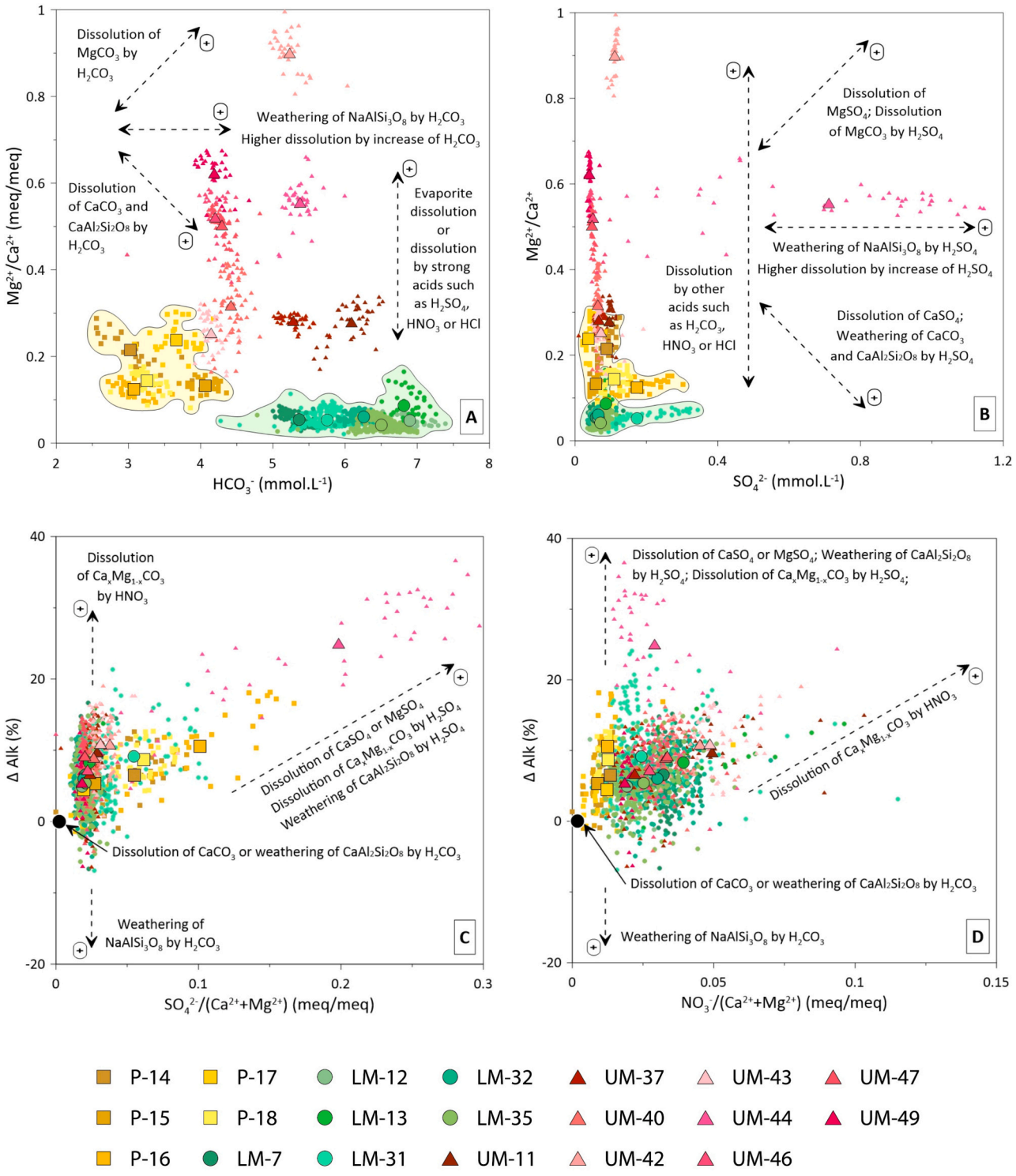

Fig. 7. Relationships between Mg^{2+}/Ca^{2+} ratio and (A) HCO_3^- and (B) SO_4^{2-}; as well as Δ Alk versus (C) $SO_4^{2-}/(Ca^{2+} + Mg^{2+})$ ratio and (D) $NO_3^-/(Ca^{2+} + Mg^{2+})$ ratio. The black dotted lines show the main weathering processes controlling the chemical composition of stream water (Liu and Han, 2021, 2020a, 2020b) (Table S1).

as high compared to the LM. Conversely, the second cluster is linked to higher pCO_2 and water temperature in the lowland areas compared to the mountain regions (Table 1).

The feedback of trends in environmental parameters —temperature, discharge, and pCO_2—on the hydrochemical trends over the last two decades was also assessed using RDA, which explained 26.5 % of the variance (RDA1, p-value <0.05) (Fig. 6B). The first axis clustered increasing trends in headwater stream discharge (p-value <0.05) and pCO_2 (p-value <0.1) in the Pyrenees and the UM, contrasting with trends observed in the LM. The second axis clustered trends in water temperature, though these were not statistically significant (Fig. 6B).

4. Discussion

4.1. Seasonal patterns on headwater chemistry

In the Pyrenees, seasonal changes in weathering processes can be linked to seasonal shifts in either calcite dissolution or anorthite hydrolysis, both driven by carbonic acid (Fig. 7A). In this region, calcite dissolution is the most plausible weathering pathway, as calcareous rocks are the predominant lithology and carbonate minerals are more soluble than silicates (Cao et al., 2012). The highest concentrations of HCO_3^- were observed around December at all study sites in this region. Previous studies in similar climatic regions, confirmed this regional pattern, showing increased carbonate dissolution between September and December, driven by the piston effect in the epikarst during the first seasonal rainfall events (Ulloa-Cedamanos et al., 2020) and the chemostatic behaviour of carbonate dissolution as discharge increases (Ulloa-Cedamanos et al., 2021a; Zeng et al., 2021).

In the UM, site 11 exhibited a clear seasonal variation in the contribution of dolomite dissolution to water chemistry. In contrast, other UM sites displayed a distribution along the vertical axis (Fig. 7A), indicating the influence of additional processes, such as mineral dissolution by strong acids. Another factor explaining this distribution is the seasonal competition between dolomite and calcite dissolution in these Mg^{2+}-rich karst catchments, which varies with flow conditions. Although the solubility of calcite is generally higher than that of dolomite, the increase in dolomite solubility is more pronounced as temperatures decrease (Drever, 1997; Szramek et al., 2007), leading to a higher potential dissolution of dolomite during the colder season.

In the LM, seasonal changes in weathering processes can be attributed to variations in albite hydrolysis, as well as fluctuations in the availability of carbonic acid or carbonate dissolution rates (Fig. 7A). Given the predominant coverage of carbonates, the hydrolysis of silicates is less likely to be a significant factor. Consequently, variations in bicarbonate concentrations are more likely related to seasonal changes in CO_2 availability in soils or to variations in stream water discharge. These hydrological variations could lead to a dilution effect in winter due to the input of less concentrated waters or an accretion effect in summer driven by higher evapotranspiration rates (Huang et al., 2018).

4.2. Strong acid disturbances

Specific sulphate patterns were observed at sites 31 in the LM, 44 in the UM, and 14, 16, and 18 in the Pyrenees. Between these sites, distribution of those in LM and Pyrenees suggests a seasonal contribution from epsomite ($MgSO_4$) dissolution and/or dolomite by sulphuric acid (Fig. 7B). The observed alkalinity loss, ranging from 6 to 11 % (Fig. 7C), supports the involvement of sulphuric acid in the dissolution processes and points to weathering of calcite by sulphuric acid as another potential source. Seasonal changes at site 44 suggest a clear variation in the availability of sulphuric acid (Fig. 7B), further supported by a significant alkalinity loss of 25 % (Fig. 7C). A common regional atmospheric source of sulphate was estimated by a $SO_4^{2-}/(Ca^{2+} + Mg^{2+})$ ratio of 0.02 in these headwater streams, confirming a minimal contribution from acid rain over the past decades (Fig. 4D). Given the minimal contribution of acid rain in the region, other sources must account for these patterns. Ulloa-Cedamanos et al. (2021b) identified sulphuric acid from pyrite (FeS_2) oxidation as a significant source of sulphates in the Pyrenean Baget catchment (site 16), which likely explains the patterns observed at other sites. Exceptionally, the high sulphate concentration at site 18 might be linked to a quarry occupying 1 km^2 of the catchment area (Fig. 1).

Nitrate inputs to surface waters originate from either biological and/or anthropogenic sources. An example of the latter is the nitrification of nitrogen fertilizers associated with agricultural activities, which is a major source of nitric acid and nitrates in stream waters (Perrin et al., 2008). Quasi-pristine sites in the Pyrenees primarily exhibited only biological inputs, as indicated by the lowest $NO_3^-/(Ca^{2+} + Mg^{2+})$ ratios (Table 1, Fig. 7D). A more detailed study at site 16 revealed that grasslands, covering 16 % of the catchment area, are used seasonally for limited livestock farming (Ulloa-Cedamanos et al., 2022). Land cover classification for this site confirmed this, showing that agricultural areas accounted for only 9.7 % of the catchment (Fig. 1). In contrast, certain sites in the Massif Central revealed a non-negligible influence from agricultural activities, evidenced by nitrate and potassium concentrations four and three times higher, respectively, than in the Pyrenees (Table 1). The first group, comprising sites 11, 12, and 43 in the UM and site 13 in the LM, demonstrated a significant agricultural impact, with $NO_3^-/(Ca^{2+} + Mg^{2+})$ ratios more than three times higher than in the Pyrenees. This observation was correlated with a loss of alkalinity exceeding 8 % (Fig. 7D) and larger areas devoted to agriculture, such as at sites 11 (46.1 %) and 13 (61.4 %) (Fig. 1). A second group, including sites 40 and 47 in the LM and sites 7 and 32 in the LM, were also affected by agriculture, though to a lesser extent. This was reflected by $NO_3^-/(Ca^{2+} + Mg^{2+})$ ratios >0.03 and significant agricultural areas, such as at sites 7 (35.8 %) and 40 (22.7 %) (Fig. 1). These results suggest that agriculture contributes to carbonate dissolution by nitric acid in this region.

4.3. Drivers on spatial patterns

Lithological input is the primary source of major elements in stream waters (Meybeck, 2003). In karst regions, water chemistry is mainly influenced by the dissolution of carbonate minerals (Calmels et al., 2014; Mangin, 1975; Mudarra and Andreo, 2010; Qin et al., 2020). In this study, the dominant carbonate mineral is calcite ($CaCO_3$), whose dissolution releases Ca^{2+} and HCO_3^- ions into water (Fig. 2), making these ions the dominant contributors to the chemical composition of stream waters. Minor lithologies (Table S1) also affect water chemistry in these headwater streams. In the UM, dolomite dissolution ($MgCO_3$) plays a non-negligeable role, resulting in high Mg^{2+} concentrations (Fig. 2), as well as high HCO_3^-/Na^+ (Fig. 4B) and Mg^{2+}/Ca^{2+} (Fig. 7A) ratios. In the Pyrenees, pyrite oxidation (FeS_2) and gypsum dissolution ($CaSO_4$) influence the water chemistry, as illustrated by the low HCO_3^-/SO_4^{2-} ratios. The contribution of these two sources to the headwater streams was confirmed in a site-specific study at site 16, using a geochemical model and stable sulphur isotope analysis (Ulloa-Cedamanos et al., 2021b). Specific water discharge was negatively associated to magnesium and sulphates (Fig. 6A). However, lithology likely plays a more dominant role in controlling these elements rather than specific water discharge alone. For instance, sites exhibiting this pattern were located in the dolomite-rich UM, with high average input of magnesium relative to calcium ($Mg^{2+}/Ca^{2+} > 0.26$) (Fig. 7A).

Meteorological conditions could contribute to hydrological differences between upland regions. Although rainfall is slightly higher in the Pyrenees compared to the UM (Moisselin et al., 2002; Pascaud et al., 2016a), the Pyrenees exhibit significantly higher drainage (Table 1). Higher drainage could potentially lead to increased carbonate dissolution by replenishing unsaturated rainwater (Huang et al., 2018) and activating a larger area of the catchment for weathering (Zeng et al., 2016). However, the results do not support this hypothesis. In the Pyrenees, higher specific discharge (Qs) is associated with lower Ca^{2+} and

HCO_3^- concentrations (Fig. 6A), attributed to a potential dilution effect and reduced contact time between water and rock during the winter rainy period (Qin et al., 2020). In LM, higher Ca^{2+} and HCO_3^- concentrations are likely due to greater evaporation processes, as supported by the lowest Qs and the highest Na^+ and Cl^- concentrations (Table 1). Despite similar environmental conditions in these upland areas, the difference in specific water discharge reveals to be a key factor explaining the observed variations in Ca^{2+} and HCO_3^- concentrations.

Water temperature and pCO_2 are clustered together, suggesting a potential synergistic effect on water chemistry patterns (Fig. 6A). Warmer conditions in the LM could indirectly increase pCO_2 levels due to enhanced organic matter production in soils, a characteristic of areas with dense vegetation. However, most sites in the Massif Central are primarily agricultural (Fig. 1), as supported by a strong relationship with nitrate concentration (Fig. 6A), particularly evident in sites 13 in LM and, 11, 42 and 44 in UM, which undermines this hypothesis. The covariation between these parameters appears to be more incidental than systematic. In warmer LM sites, agricultural activities cause soil erosion, releasing soil carbon (Holz and Augustin, 2021; Kwang et al., 2023; Ponnou-Delaffon et al., 2020) and potentially raising pCO_2 concentrations in streams. Despite higher pCO_2 concentrations, stronger acids would interfere with carbonate dissolution in the Massif Central. Several studies show that headwaters oversaturated with CO_2 tends to release it within the first hundred meters downstream (Johnson et al., 2008). This carbon process is likely to occur in this region, with much higher rates of CO_2 emission in UM due to the steep topography (Rocher-Ros et al., 2019).

4.4. Environmental feedback on hydrochemical trends

The increase in pCO_2 has been linked to various anthropogenic activities (Jeannin et al., 2016; Stets et al., 2014), but it is also an indicator of reforestation (Ek and Godissart, 2014; Ulloa-Cedamanos et al., 2022). In the Pyrenees, increasing CO_2 trends are accompanied by negative NO_3^- trends, suggesting a continued decline in seasonal agricultural activities, a pattern observed at site 16 (Ulloa-Cedamanos et al., 2022) and other Pyrenean regions (Khorchani et al., 2020). In contrast, UM sites exhibit increasing NO_3^- trends in areas with minimal agricultural activity (e.g., 23 % of catchment surface at site 40, Fig. 1). The only UM site with a decreasing NO_3^- trend (site 11) already has a substantial agricultural footprint (site 11, 46 %). These patterns suggest that nitric acid is becoming more influential in less anthropized catchments in UM.

Trends in Ca^{2+} and Mg^{2+} concentration were inversely related to increasing pCO_2 and discharge trends (Fig. 6B). The contribution of these ions to the RDA axis is linked to significant positive trends in the LM, whereas trends in other regions were rarely significant for these elements (Table S3). This suggests that the observed increase in Ca^{2+} and Mg^{2+} concentrations in the LM occurred within the context of decreasing water discharge and pCO_2. The decrease in water discharge could result in lower rainwater dilutions of Ca^{2+} and Mg^{2+} (Fig. 6B). This hypothesis is further supported by a trend of increasing dissolved element concentrations across the region (Table S2). The simultaneous rise in these ions and decrease in pCO_2 points out the involvement of another source of acidity, potentially sulphuric acid, which can promote mineral weathering. However, sulphate concentrations showed a consistent downward trend (Table S2), reflecting the significant reduction in atmospheric acid deposition (Coddeville et al., 2016; Pascaud et al., 2016a; Pierret et al., 2019), which has declined by 65 % between 1990 and 2009 (Monks et al., 2009). Given that SO_4^{2-} concentrations regionally decreased (except at site 18, Fig. 5), the hypothesis that nitric acid, rather than sulphuric acid, is the dominant source of acidity, as seen in other regions of France (Probst and Ambroise, 2019), gains further support. However, NO_3^- concentration trends were variable across the LM (Table S3). A temporal analysis of land-use change would be valuable for confirming the growing role of nitric acid in rock weathering in these carbonate environments (Ulloa-Cedamanos et al., 2022). This is particularly important given that nitric acid may be replacing the declining influence of sulphuric acid from acid rain (Pascaud et al., 2016b; Pierret et al., 2019).

Although most sites indicated an increasing trend in temperature (Table S2), only a few showed significant trends (Table S3). Water temperature in karst systems tends to be stable, as it reflects the equilibrium between groundwater stored in the karst and the stable ground temperature. This inherent stability suggests that a higher frequency of measurements over medium- to long-term monitoring is necessary to detect significant trends. While the observed increase in water temperature may not always be statistically significant in this study, numerous studies have highlighted the impact of global warming on air temperature and water chemistry in France and globally (Binet et al., 2020; Gaillardet et al., 2019; IPCC, 2014; Labat et al., 2004; Ponnou-Delaffon et al., 2020; Ulloa-Cedamanos et al., 2020; Zeng et al., 2021).

4.5. Regional and global implications

Hydrological conditions, regardless of geographical location, drive seasonal changes in karst headwater streams in this temperate region. This finding has significant implications in the context of global change. Anticipated shifts in seasonal drainage patterns—such as earlier or later rain events and more frequent extreme weather events (IPCC, 2021)—are expected to alter current seasonal variations. Initially, increased discharge would enhance dissolved element concentrations due to intensified chemical weathering, but sustained or sudden rises in discharge would reduce water-rock contact time, ultimately decreasing weathering rates (Zeng et al., 2016).

Karst headwaters in both lowland and upland areas of the Massif Central feature catchments with extensive agricultural coverage. This anthropogenic activity generates nitric acid, which competes with carbonic acid in driving chemical weathering (Perrin et al., 2008). Sulphuric acid from atmospheric deposition is no longer prevalent, as indicated by the consistent decline in sulphate concentrations. With less CO_2 consumed in carbonate dissolution, more CO_2 can accumulate and reach saturation. These saturated waters may become hotspots for CO_2 emissions, particularly in upland headwaters where steep topography enhances turbulence (Rocher-Ros et al., 2019).

Although land cover differs in upland regions, both exhibit rising pCO_2 trends in these headwater streams. In the Pyrenees, a clear reforestation trend is observed (García-Ruiz and Lana-Renault, 2011; López-Moreno et al., 2011; Ulloa-Cedamanos et al., 2022), while increasing NO_3^- trends in the UM suggest growing agricultural activities. This is particularly significant as land use in upland regions is changing in Europe (Rabbinge and van Diepen, 2000) and globally (Reed et al., 2009; Winkler et al., 2021), indicating that rising pCO_2 trends from these land use shifts are expected. This process and its future evolution must be accounted for in the global carbon budget (Friedlingstein et al., 2023), and carbon-related policies should be updated accordingly. Although headwater streams occupy small areas, they are abundant across river networks, especially in karst systems. Upland headwater streams are already recognized as hotspots for CO_2 emissions globally (Ågren et al., 2007; Marx et al., 2017; Wallin et al., 2018). The rising pCO_2 levels suggest even higher CO_2 emission rates to be expected in these regions. Including land-use changes in this equation underscores the greater significance of upland regions in the global carbon cycle.

Drier conditions in the LM could have regional implications, such as rising Ca^{2+}+Mg^{2+} concentration trends in headwater streams. However, this trend also raises concerns about future water security since climate projections for the end of the 21st century suggest a reduced runoff generation because of less precipitation in this region (García-Ruiz et al., 2011; López-Moreno et al., 2011). Agricultural activities demand large amounts of water (Cudennec et al., 2007; Ho et al., 2016), often sourced from karstic groundwater systems. If water usage exceeds groundwater replenishment over time, springs could dry up, particularly during the summer months, impacting human water supply.

Headwater streams in the Massif Central are largely covered by agricultural areas, but pCO_2 trends differ between uplands and lowlands. This pattern is accompanied by mixed increasing and decreasing NO_3^- trends in the lowlands. Investigating land-use change is crucial for understanding these trends, likely linked to the historical evolution of these areas (Dusseux, 2014; Guerschman et al., 2003). The frequency and intensity of agricultural activities also vary between the regions. In the uplands, the challenging topography limits intensive agriculture, favouring livestock farming, while lowlands would have a longer history of intensive agriculture (Camacho et al., 2008; Génot and Schnitzler, 2012; Pointereau and Coulon, 2009).

5. Conclusions

This study analyzed the relationship between changes in water chemistry and environmental factors across twenty karst catchments in the Pyrenees and the low (LM) and uplands (UM) in the Massif Central over the last two decades. The catchments were grouped into three clusters based on hydrological and hydrochemical profiles. Despite geographical distance, UM and Pyrenean sites exhibited strong similarities. However, minor lithological inputs along with variations in pCO_2 and hydrological conditions, shaped the unique chemical signatures of each region. Seasonal changes in water chemistry were primarily driven by hydrological conditions across karst headwaters. Additionally, lithology, such as dolomite in UM and pyrite and gypsum in the Pyrenees, contributed to seasonal variations in Mg^{2+} and SO_4^{2-}, respectively. An atmospheric source for SO_4^{2-} was ruled out due to decreasing SO_4^{2-} trends over the past two decades, aligning with confirmed reductions in atmospheric acid deposition in the region. Land use also played a critical role, with agricultural practices increasing NO_3^- and indirectly elevating pCO_2 concentrations in the Massif Central.

The observed trends have regional and global implications. Rising pCO_2 trends in uplands revealed a common consequence from two antagonist land uses: reforestation in the Pyrenees, and ongoing agricultural practices in UM, the latter pointed out by increasing NO_3^- concentration trends. These rising pCO_2 levels in headwater streams, particularly in steep uplands, have significant consequences for the carbon cycle, given that such streams are CO_2 emission hotspots. However, the scarcity of direct observations in these ecosystems introduces large uncertainties in both current and future global carbon budgets. These uncertainties are exacerbated by the rapid changes in land use, which further complicate projections of CO_2 emissions. This study demonstrates that under varying land uses, pCO_2 concentrations are rising in upland karst headwaters, with high potential for emissions. Such findings should be incorporated into regional carbon budgets and inform updates to carbon-related policies. The decreasing trend in water discharge is likely responsible for rising cation concentrations in lowlands in Massif Central. This decrease in water resource also poses challenges for water resource management in a region where karst groundwater supports both irrigation and water supply.

By integrating spatial and temporal analyses, this study offers a comprehensive understanding of how karst headwaters respond to land use changes and hydrological variations, providing a crucial baseline for predicting future shifts in water chemistry and carbon dynamics in similar regions globally. Future studies should prioritize long-term, high-frequency monitoring to capture interannual and seasonal variations, as well as finer-scale events such as diel changes or floods, which are expected to become more frequent and intense. Expanding this research to karst systems worldwide, across different climatic zones, will help validate the broader applicability of these findings, contribute to a deeper understanding of global carbon cycles and water resource management in a changing environment, and support model development.

CRediT authorship contribution statement

F. Ulloa-Cedamanos: Writing – original draft, Visualization, Validation, Software, Resources, Methodology, Investigation, Formal analysis, Data curation, Conceptualization. **J.L. Probst:** Writing – review & editing, Validation, Supervision, Project administration, Methodology, Investigation, Funding acquisition, Conceptualization. **A. Probst:** Writing – review & editing, Validation, Supervision, Project administration, Methodology, Investigation, Funding acquisition, Conceptualization.

Funding

This research was supported by the CNRS-INSU within the framework of the SNO Karst and IR OZCAR and by the CNRS-INEE within the framework of the LTSER Zone Atelier Pyrenees-Garonne (LTSER ZA PYGAR), which is part of the IR RZA.

Declaration of competing interest

The authors declare that they have no known competing financial interests or personal relationships that could have appeared to influence the work reported in this paper.

Acknowledgments

The BC belongs to the French Karst Network (SNO Karst, Jourde et al., 2018; www.sokarst.org) initiative of the INSU/CNRS, which aims to strengthen knowledge-sharing and to promote cross-disciplinary research on karst systems. It is one of the observatories of the French Research Infrastructure called OZCAR (the French network of Critical Zone Observatories, Gaillardet et al., 2018) and also a LTSER (Long-Term Socio-Ecological Research) research site of the CNRS (National Center for Scientific Research) collaborative research platform called "Zone Atelier Pyrénées-Garonne (ZA PYGAR)", which is part of a French Research Infrastructure called RZA (Réseau des Zones Ateliers, Bretagnolle et al., 2019). RZA grouped with OZCAR is the French contribution to the European Research Infrastructure eLTER (Long-Term Ecosystem in Europe, Mirtl et al., 2018). The authors specially thank the support from CNRS INEE and INSU, SNO KARST, OZCAR and Zone Atelier Pyrénées-Garonne (LTSER ZA PYGAR), and of the Ades and hydroportail data bases.

F. Ulloa-Cedamanos's PhD was supported by a fellowship from the French Ministry of Higher Education, Research and Innovation.

Appendix A. Supplementary data

Supplementary data to this article can be found online at https://doi.org/10.1016/j.scitotenv.2024.177614.

Data availability

Data will be made available on request.

References

ADES database, 2024. Accès aux données [WWW Document]. https://ades.eaufrance.fr/Recherche (accessed 5.24.24).

Ågren, A., Buffam, I., Jansson, M., Laudon, H., 2007. Importance of seasonality and small streams for the landscape regulation of dissolved organic carbon export. Eur. J. Vasc. Endovasc. Surg. 112. https://doi.org/10.1029/2006JG000381.

Amiotte Suchet, P., Probst, J.-L., 1995. A global model for present day atmospheric/soil CO2 consumption by chemical erosion of continental rocks (GEM-CO2). Tellus Ser. B 47, 273–280.

Amiotte Suchet, P., Probst, J.-L., 1996. Origines du carbone inorganique dissous dans les eaux de la Garonne. Variations saisonnières et interannuelles. Sci. Géologiques 49, 101–126. https://doi.org/10.3406/sgeol.1996.1938.

Amiotte Suchet, P., Probst, J.-L., Ludwig, W., 2003. Worldwide distribution of continental rock lithology: implications for the atmospheric/soil CO2 uptake by continental weathering and alkalinity river transport to the oceans. Glob. Biogeochem. Cycles 17, 1038. https://doi.org/10.1029/2002gb001891.

Bauer, J.E., Cai, W.-J., Raymond, P.A., Bianchi, T.S., Hopkinson, C.S., Regnier, P.A.G., 2013. The changing carbon cycle of the coastal ocean. Nature 504, 61–70. https://doi.org/10.1038/nature12857.

Binet, S., Probst, J.L., Batiot, C., Seidel, J.L., Emblanch, C., Peyraube, N., Charlier, J.-B., Bakalowicz, M., Probst, A., 2020. Global warming and acid atmospheric deposition impacts on carbonate dissolution and CO2 fluxes in French karst hydrosystems: evidence from hydrochemical monitoring in recent decades. Geochim. Cosmochim. Acta 270, 184–200. https://doi.org/10.1016/J.GCA.2019.11.021.

Bretagnolle, V., Benoit, M., Bonnefond, M., Breton, V., Church, J.M., Gaba, S., Gilbert, D., Gillet, F., Glatron, S., Guerbois, C., Lamouroux, N., Lebouvier, M., Mazé, C., Mouchel, J.M., Ouin, A., Pays, O., Piscart, C., Ragueneau, O., Servain, S., Spiegelberger, T., Fritz, H., 2019. Action-orientated research and framework: insights from the French longterm social-ecological research network. Ecol. Soc. 24. https://doi.org/10.5751/ES-10989-240310.

Brunet, R., Coppolani, J., 1970. Atlas Midi-Pyrenees. Berger-Levrault.

Calmels, D., Gaillardet, J., François, L., 2014. Sensitivity of carbonate weathering to soil CO2 production by biological activity along a temperate climate transect. Chem. Geol. 390, 74–86. https://doi.org/10.1016/j.chemgeo.2014.10.010.

Camacho, O., Dobremez, L., Capillon, A., 2008. Des broussailles dans les prairies alpines. Rev. Geogr. Alp. 77–88. https://doi.org/10.4000/rga.566.

Cao, J., Yuan, D., Groves, C., Huang, F., Yang, H., Lu, Q., 2012. Carbon fluxes and sinks: the consumption of atmospheric and soil CO2 by carbonate rock dissolution. Acta Geologica Sinica - English Edition 86, 963–972. https://doi.org/10.1111/j.1755-6724.2012.00720.x.

Chen, Z., Auler, A.S., Bakalowicz, M., Drew, D., Griger, F., Hartmann, J., Jiang, G., Moosdorf, N., Richts, A., Stevanovic, Z., Veni, G., Goldscheider, N., 2017. The world karst aquifer mapping project: concept, mapping procedure and map of Europe. Hydrogeol. J. 25, 771–785. https://doi.org/10.1007/s10040-016-1519-3.

Cloutier, V., Lefebvre, R., Therrien, R., Savard, M.M., 2008. Multivariate statistical analysis of geochemical data as indicative of the hydrogeochemical evolution of groundwater in a sedimentary rock aquifer system. J. Hydrol. (Amst) 353, 294–313. https://doi.org/10.1016/J.JHYDROL.2008.02.015.

Coddeville, P., Nicolas, M., Mathias, E., Pascaud, A., Sauvage, S., Probst, A., 2016. Évolution des émissions, de la qualité de l'air et des dépôts atmosphériques dans les espaces ruraux (forestiers). Pollution atmosphérique 229–230. https://doi.org/10.4267/pollution-atmospherique.

Cole, J.J., Prairie, Y.T., Caraco, N.F., McDowell, W.H., Tranvik, L.J., Striegl, R.G., Duarte, C.M., Kortelainen, P., Downing, J.A., Middelburg, J.J., Melack, J., 2007. Plumbing the global carbon cycle: integrating inland waters into the terrestrial carbon budget. Ecosystems 10, 171–184. https://doi.org/10.1007/s10021-006-9013-8.

Coxon, C., 2011. Agriculture and karst. In: van Beynen, P. (Ed.), Karst Management. Springer, Dordrecht, pp. 103–138.

Cudennec, C., Leduc, C., Koutsoyiannis, D., 2007. Dryland hydrology in Mediterranean regions—a review. Hydrol. Sci. J. 52, 1077–1087. https://doi.org/10.1623/hysj.52.6.1077.

Drever, J.I., 1997. The Geochemistry of Natural Waters, Surface and Groundwater Environments, Third, edit. ed. Upper Saddle River, NJ.

Dreybrodt, W., 1988. Processes in Karst Systems. Springer, Heidelberg, Germany.

Dusseux, P., 2014. Exploitation de séries temporelles d'images satellites à haute résolution spatiale pour le suivi des prairies en milieu agricole (Ph.D Tesis). Université Rennes 2, France.

Eau France, 2024. Hydro Portail v3.1.4.3 [WWW Document]. URL. https://www.hydro.eaufrance.fr/rechercher/entites-hydrometriques (accessed 5.24.24).

Ek, C., Godissart, J., 2014. Carbon dioxide in cave air and soil air in some karstic areas of Belgium. A prospective view. Geol. Belg. 17, 102–106.

Etchanchu, D., Probst, J.L., 1988. Evolution de la composition chimique des eaux de la garonne entre 1971 et 1984. Hydrol. Sci. J. 33, 243–256. https://doi.org/10.1080/02626668809491246.

Ford, D., Williams, P., 2007. Karst Hydrogeology and Geomorphology, Karst hydrogeology and geomorphology. https://doi.org/10.1002/9781118684986.

Forester, B.R., Lasky, J.R., Wagner, H.H., Urban, D.L., 2018. Comparing methods for detecting multilocus adaptation with multivariate genotype–environment associations. Mol. Ecol. 27, 2215–2233. https://doi.org/10.1111/mec.14584.

Friedlingstein, P., O'Sullivan, M., Jones, M.W., Andrew, R.M., Bakker, D.C.E., Hauck, J., Landschützer, P., Le Quéré, C., Luijkx, I.T., Peters, G.P., Peters, W., Pongratz, J., Schwingshackl, C., Sitch, S., Canadell, J.G., Ciais, P., Jackson, R.B., Alin, S.R., Anthoni, P., Barbero, L., Bates, N.R., Becker, M., Bellouin, N., Decharme, B., Bopp, L., Brasika, I.B.M., Cadule, P., Chamberlain, M.A., Chandra, N., Chau, T.-T.-T., Chevallier, F., Chini, L.P., Cronin, M., Dou, X., Enyo, K., Evans, W., Falk, S., Feely, R. A., Feng, L., Ford, D.J., Gasser, T., Ghattas, J., Gkritzalis, T., Grassi, G., Gregor, L., Gruber, N., Gürses, Ö., Harris, I., Hefner, M., Heinke, J., Houghton, R.A., Hurtt, G.C., Iida, Y., Ilyina, T., Jacobson, A.R., Jain, A., Jarníková, T., Jersild, A., Jiang, F., Jin, Z., Joos, F., Kato, E., Keeling, R.F., Kennedy, D., Klein Goldewijk, K., Knauer, J., Korsbakken, J.I., Körtzinger, A., Lan, X., Lefèvre, N., Li, H., Liu, J., Liu, Z., Ma, L., Marland, G., Mayot, N., McGuire, P.C., McKinley, G.A., Meyer, G., Morgan, E.J., Munro, D.R., Nakaoka, S.-I., Niwa, Y., O'Brien, K.M., Olsen, A., Omar, A.M., Ono, T., Paulsen, M., Pierrot, D., Pocock, K., Poulter, B., Powis, C.M., Rehder, G., Resplandy, L., Robertson, E., Rödenbeck, C., Rosan, T.M., Schwinger, J., Séférian, R., Smallman, T.L., Smith, S.M., Sospedra-Alfonso, R., Sun, Q., Sutton, A.J., Sweeney, C., Takao, S., Tans, P.P., Tian, H., Tilbrook, B., Tsujino, H., Tubiello, F., van der Werf, G. R., van Ooijen, E., Wanninkhof, R., Watanabe, M., Wimart-Rousseau, C., Yang, D., Yang, X., Yuan, W., Yue, X., Zaehle, S., Zeng, J., Zheng, B., 2023. Global carbon budget 2023. Earth Syst. Sci. Data 15, 5301–5369. https://doi.org/10.5194/essd-15-5301-2023.

Gaillardet, J., Dupre, B., Louvat, P., Allegre, C.J., 1999. Global silicate weathering and CO2 consumption rates deduced from the chemistry of large rivers. Chem. Geol. 159, 3–30. https://doi.org/10.1016/S0009-2541(99)00031-5.

Gaillardet, J., Braud, I., Hankard, F., Anquetin, S., Bour, O., Dorfliger, N., de Dreuzy, J.R., Galle, S., Galy, C., Gogo, S., Gourcy, L., Habets, F., Laggoun, F., Longuevergne, L., Le Borgne, T., Naaim-Bouvet, F., Nord, G., Simonneaux, V., Six, D., Tallec, T., Valentin, C., Abril, G., Allemand, P., Arènes, A., Arfib, B., Arnaud, L., Arnaud, N., Arnaud, P., Audry, S., Comte, V.B., Batiot, C., Battais, A., Bellot, H., Bernard, E., Bertrand, C., Bessière, H., Binet, S., Bodin, J., Bodin, X., Boithias, L., Bouchez, J., Boudevillain, B., Moussa, I.B., Branger, F., Braun, J.J., Brunet, P., Caceres, B., Calmels, D., Cappelaere, B., Celle-Jeanton, H., Chabaux, F., Chalikakis, K., Champollion, C., Copard, Y., Cotel, C., Davy, P., Deline, P., Delrieu, G., Demarty, J., Dessert, C., Dumont, M., Emblanch, C., Ezzahar, J., Estèves, M., Favier, V., Faucheux, M., Filizola, N., Flammarion, P., Floury, P., Fovet, O., Fournier, M., Francez, A.J., Gandois, L., Gascuel, C., Gayer, E., Genthon, C., Gérard, M.F., Gilbert, D., Gouttevin, I., Grippa, M., Gruau, G., Jardani, A., Jeanneau, L., Join, J.L., Jourde, H., Karbou, F., Labat, D., Lagadeuc, Y., Lajeunesse, E., Lastennet, R., Lavado, W., Lawin, E., Lebel, T., Le Bouteiller, C., Legout, C., Lejeune, Y., Le Meur, E., Le Moigne, N., Lions, J., Lucas, A., Malet, J.P., Marais-Sicre, C., Maréchal, J.C., Marlin, C., Martin, P., Martins, J., Martinez, J.M., Massei, N., Mauclerc, A., Mazzilli, N., Molénat, J., Moreira-Turcq, P., Mougin, E., Morin, S., Ngoupayou, J.N., Panthou, G., Peugeot, C., Picard, G., Pierret, M.C., Porel, G., Probst, A., Probst, J.L., Rabatel, A., Raclot, D., Ravanel, L., Rejiba, F., René, P., Ribolzi, O., Riotte, J., Rivière, A., Robain, H., Ruiz, L., Sanchez-Perez, J.M., Santini, W., Sauvage, S., Schoeneich, P., Seidel, J.L., Sekhar, M., Sengtaheuanghoung, O., Silvera, N., Steinmann, M., Soruco, A., Tallec, G., Thibert, E., Lao, D.V., Vincent, C., Viville, D., Wagnon, P., Zitouna, R., 2018. OZCAR: the French network of critical zone observatories. Vadose Zone J. 17, 1–24. https://doi.org/10.2136/vzj2018.04.0067.

Gaillardet, J., Calmels, D., Romero-Mujalli, G., Zakharova, E., Hartmann, J., 2019. Global climate control on carbonate weathering intensity. Chem. Geol. 527, 118762. https://doi.org/10.1016/j.chemgeo.2018.05.009.

Gandois, L., Agnan, Y., Leblond, S., Séjalon-Delmas, N., Le Roux, G., Probst, A., 2014. Use of geochemical signatures, including rare earth elements, in mosses and lichens to assess spatial integration and the influence of forest environment. Atmos. Environ. 95, 96–104. https://doi.org/10.1016/j.atmosenv.2014.06.029.

García-Ruiz, J.M., Lana-Renault, N., 2011. Hydrological and erosive consequences of farmland abandonment in Europe, with special reference to the Mediterranean region – a review. Agric. Ecosyst. Environ. 140, 317–338. https://doi.org/10.1016/J.AGEE.2011.01.003.

García-Ruiz, J.M., López-Moreno, J.I., Vicente-Serrano, S.M., Lasanta-Martínez, T., Beguería, S., 2011. Mediterranean water resources in a global change scenario. Earth Sci. Rev. 105, 121–139. https://doi.org/10.1016/J.EARSCIREV.2011.01.006.

Garrels, R.M., Mackenzie, F.T., 1971. Evolution of Sedimentary Rocks. Norton, New York, N.Y.

Génot, J.-C., Schnitzler, A., 2012. La France des friches. In: De la ruralité à la féralité, Matière à débattre et décider. Éditions Quæ, Versailles.

Gislason, S.R., Oelkers, E.H., Eiriksdottir, E.S., Kardjilov, M.I., Gisladottir, G., Sigfusson, B., Snorrason, A., Elefsen, S., Hardardottir, J., Torssander, P., Oskarsson, N., 2009. Direct evidence of the feedback between climate and weathering. Earth Planet. Sci. Lett. 277, 213–222. https://doi.org/10.1016/j.epsl.2008.10.018.

Goldscheider, N., Chen, Z., Auler, A.S., Bakalowicz, M., Broda, S., Drew, D., Hartmann, J., Jiang, G., Moosdorf, N., Stevanovic, Z., Veni, G., 2020. Global distribution of carbonate rocks and karst water resources. Hydrogeol. J. 28, 1661–1677. https://doi.org/10.1007/s10040-020-02139-5/Published.

Grusson, Y., 2016. Modelisation De L'Evolution Hydroclimatique Des Flux Et Stocks D'Eau Verte Et D'Eau Bleue Du Bassin Versant De La Garonne (PhD thesis). Toulouse INP, Toulouse.

Guerschman, J.P., Paruelo, J.M., Di Bella, C., Giallorenzi, M.C., Pacin, F., 2003. Land cover classification in the argentine pampas using multi-temporal Landsat TM data. Int. J. Remote Sens. 24, 3381–3402. https://doi.org/10.1080/0143116021000021288.

Gwiazda, R.H., Broecker, W.S., 1994. The separate and combined effects of temperature, soilpCO2, and organic acidity on silicate weathering in the soil environment: formulation of a model and results. Glob. Biogeochem. Cycles 8, 141–155. https://doi.org/10.1029/94GB00491.

Ho, M., Parthasarathy, V., Etienne, E., Russo, T.A., Devineni, N., Lall, U., 2016. America's water: agricultural water demands and the response of groundwater. Geophys. Res. Lett. 43, 7546–7555. https://doi.org/10.1002/2016GL069797.

Holz, M., Augustin, J., 2021. Erosion effects on soil carbon and nitrogen dynamics on cultivated slopes: a meta-analysis. Geoderma 397, 115045. https://doi.org/10.1016/j.geoderma.2021.115045.

Huang, X., Fang, N.F., Zhu, T.X., Wang, L., Shi, Z.H., Hua, L., 2018. Hydrological response of a large-scale mountainous watershed to rainstorm spatial patterns and reforestation in subtropical China. Sci. Total Environ. 645, 1083–1093. https://doi.org/10.1016/j.scitotenv.2018.07.248.

IPCC, 2014. Climate change 2014: Synthesis report. Contribution of working groups I. In: II and III to the Fifth Assessment Report of the Intergovernmental Panel on Climate Change, Ipcc. IPCC, Geneva, Switzerland. https://doi.org/10.1046/j.1365-2559.2002.1340a.x.

IPCC, 2021. Climate Change 2021. The Physical Science Basis. Contribution of Working Group I to the Sixth Assessment Report of the Intergovernmental Panel on Climate Change. Cambridge University Press.

Jeannin, P.-Y., Hessenauer, M., Malard, A., Chapuis, V., 2016. Impact of global change on karst groundwater mineralization in the Jura Mountains. Sci. Total Environ. 541, 1208–1221. https://doi.org/10.1016/J.SCITOTENV.2015.10.008.

Johnson, M.S., Lehmann, J., Riha, S.J., Krusche, A.V., Richey, J.E., Ometto, J.P.H.B., Couto, E.G., 2008. CO2 efflux from Amazonian headwater streams represents a significant fate for deep soil respiration. Geophys. Res. Lett. 35. https://doi.org/10.1029/2008GL034619.

Jourde, H., Massei, N., Mazzilli, N., Binet, S., Batiot-Guilhe, C., Labat, D., Steinmann, M., Bailly-Comte, V., Seidel, J.L., Arfib, B., Charlier, J.B., Guinot, V., Jardani, A., Fournier, M., Aliouache, M., Babic, M., Bertrand, C., Brunet, P., Boyer, J.F., Bricquet, J.P., Camboulive, T., Carrière, S.D., Celle-Jeanton, H., Chalikakis, K., Chen, N., Cholet, C., Clauzon, V., Dal Soglio, L., Danquigny, C., Défargue, C., Denimal, S., Emblanch, C., Hernandez, F., Gillon, M., Gutierrez, A., Hidalgo Sanchez, L., Hery, M., Houillon, N., Johannet, A., Jouves, J., Jozja, N., Ladouche, B., Leonardi, V., Lorette, G., Loup, C., Marchand, P., de Montety, V., Muller, R., Ollivier, C., Sivelle, V., Lastennet, R., Lecoq, N., Maréchal, J.C., Perotin, L., Perrin, J., Petre, M.A., Peyraube, N., Pistre, S., Plagnes, V., Probst, A., Probst, J.-L., Simler, R., Stefani, V., Valdes-Lao, D., Viseur, S., Wang, X., 2018. SNO KARST: a french network of observatories for the multidisciplinary study of critical zone processes in karst watersheds and aquifers. Vadose Zone J. 17. https://doi.org/10.2136/vzj2018.04.0094.

Kaiser, H.F., 1958. The varimax criterion for analytic rotation in factor analysis. Psychometrika 23, 187–200. https://doi.org/10.1007/BF02289233.

Kessler, J., Chambraud, A., 1990. Météo de la France: tous les climats localité par localité. J.C, Lattès, France.

Khorchani, M., Nadal-Romero, E., Tague, C., Lasanta, T., Zabalza, J., Lana-Renault, N., Domínguez-Castro, F., Choate, J., 2020. Effects of active and passive land use management after cropland abandonment on water and vegetation dynamics in the central Spanish Pyrenees. Sci. Total Environ. 717, 137160. https://doi.org/10.1016/j.scitotenv.2020.137160.

Kwang, J.S., Thaler, E.A., Larsen, I.J., 2023. The future of soils in the Midwestern United States. Earths. Future 11, e2022EF003104. https://doi.org/10.1029/2022EF003104.

Labat, D., Goddéris, Y., Probst, J.-L., Guyot, J.L., 2004. Evidence for global runoff increase related to climate warming. Adv. Water Resour. 27, 631–642. https://doi.org/10.1016/J.ADVWATRES.2004.02.020.

Laffitte, P., 1972. Traité d'informatique géologique, 624 p. : ill.; 25 cm.

Lechuga-Crespo, J.L., Sánchez-Pérez, J.M., Sauvage, S., Hartmann, J., Amiotte Suchet, P., Probst, J.L., Ruiz-Romera, E., 2020. A model for evaluating continental chemical weathering from riverine transports of dissolved major elements at a global scale. Glob. Planet. Chang. 192, 103226. https://doi.org/10.1016/j.gloplacha.2020.103226.

Legendre, P., Legendre, L., 2012. Numerical Ecology, 3rd Editio. ed. Elsevier.

Li, L., 2019. Watershed Reactive Transport. Rev. Mineral. Geochem. 85, 381–418. https://doi.org/10.2138/rmg.2018.85.13.

Liu, J., Han, G., 2020a. Effects of chemical weathering and CO2 outgassing on δ13CDIC signals in a karst watershed. J. Hydrol. (Amst) 589, 125192. https://doi.org/10.1016/j.jhydrol.2020.125192.

Liu, J., Han, G., 2020b. Major ions and δ34SSO4 in Jiulongjiang River water: investigating the relationships between natural chemical weathering and human perturbations. Sci. Total Environ. 724, 138208. https://doi.org/10.1016/j.scitotenv.2020.138208.

Liu, J., Han, G., 2021. Tracing riverine sulfate source in an agricultural watershed : constraints from stable isotopes ☆. Environ. Pollut. 288, 117740. https://doi.org/10.1016/j.envpol.2021.117740.

Liu, M., Raymond, P.A., Lauerwald, R., Zhang, Q., Trapp-Müller, G., Davis, K.L., Moosdorf, N., Xiao, C., Middelburg, J.J., Bouwman, A.F., Beusen, A.H.W., Peng, C., Lacroix, F., Tian, H., Wang, J., Li, M., Zhu, Q., Cohen, S., van Hoek, W.J., Li, Ya, Li, Yangmingkai, Yao, Y., Regnier, P., 2024. Global riverine land-to-ocean carbon export constrained by observations and multi-model assessment. Nat. Geosci. 17, 896–904. https://doi.org/10.1038/s41561-024-01524-z.

Liu, Z., Macpherson, G.L., Groves, C., Martin, J.B., Yuan, D., Zeng, S., 2018. Large and active CO2 uptake by coupled carbonate weathering. Earth Sci. Rev. 182, 42–49. https://doi.org/10.1016/J.EARSCIREV.2018.05.007.

López-Moreno, J.I., Vicente-Serrano, S.M., Moran-Tejeda, E., Zabalza, J., Lorenzo-Lacruz, J., García-Ruiz, J.M., 2011. Impact of climate evolution and land use changes on water yield in the Ebro basin. Hydrol. Earth Syst. Sci. 15, 311–322. https://doi.org/10.5194/hess-15-311-2011.

Macpherson, G.L., Sullivan, P.L., 2019. Watershed-scale chemical weathering in a merokarst terrain, northeastern Kansas, USA. Chem. Geol. 527, 118988. https://doi.org/10.1016/j.chemgeo.2018.12.001.

Mangin, A., 1975. Contribution à l'étude hydrodynamique des aquifères karstiques (Ann. Spéléo., 1974 29: 283-332; 1974 29: 495-601; 1975 30: 21-124).

Marx, A., Dusek, J., Jankovec, J., Sanda, M., Vogel, T., van Geldern, R., Hartmann, J., Barth, J.A.C., 2017. A review of CO2 and associated carbon dynamics in headwater streams: a global perspective. Rev. Geophys. 55, 560–585. https://doi.org/10.1002/2016RG000547.

Meersmans, J., Martin, M.P., Lacarce, E., De Baets, S., Jolivet, C., Boulonne, L., Lehmann, S., Saby, N.P.A., Bispo, A., Arrouays, D., 2012. A high resolution map of French soil organic carbon. Agron. Sustain. Dev. 32, 841–851. https://doi.org/10.1007/s13593-012-0086-9.

Meybeck, M., 2003. 5.08 - Global Occurrence of Major Elements in Rivers. In: Holland, H.D., Turekian, K.K.B.T.-T., on G. (Eds.), Pergamon, Oxford, pp. 207–224. https://doi.org/10.1016/B0-08-043751-6/05164-1.

Mirtl, M., Borer, E., T., Djukic, I., Forsius, M., Haubold, H., Hugo, W., Jourdan, J., Lindenmayer, D., McDowell, W.H., Muraoka, H., Orenstein, D.E., Pauw, J.C., Peterseil, J., Shibata, H., Wohner, C., Yu, X., Haase, P., 2018. Genesis, goals and achievements of long-term ecological research at the global scale: a critical review of ILTER and future directions. Sci. Total Environ. 626, 1439–1462. https://doi.org/10.1016/j.scitotenv.2017.12.001.

Moisselin, J.-M., Schneider, M., CAanellas, C., Mestre, O., 2002. Les changements climatiques en France au XXè siècle. Etude des longues séries homogénéisées de données de température et de précipitations. La Météorologie 38, 45–56. https://doi.org/10.4267/2042/36233.

Monks, P.S., Granier, C., Fuzzi, S., Stohl, A., Williams, M.L., Akimoto, H., Amann, M., Baklanov, A., Baltensperger, U., Bey, I., Blake, N., Blake, R.S., Carslaw, K., Cooper, O.R., Dentener, F., Fowler, D., Fragkou, E., Frost, G.J., Generoso, S., Ginoux, P., Grewe, V., Guenther, A., Hansson, H.C., Henne, S., Hjorth, J., Hofzumahaus, A., Huntrieser, H., Isaksen, I.S.A., Jenkin, M.E., Kaiser, J., Kanakidou, M., Klimont, Z., Kulmala, M., Laj, P., Lawrence, M.G., Lee, J.D., Liousse, C., Maione, M., McFiggans, G., Metzger, A., Mieville, A., Moussiopoulos, N., Orlando, J.J., O'Dowd, C.D., Palmer, P.I., Parrish, D.D., Petzold, A., Platt, U., Pöschl, U., Prévôt, A.S.H., Reeves, C.E., Reimann, S., Rudich, Y., Sellegri, K., Steinbrecher, R., Simpson, D., ten Brink, H., Theloke, J., van der Werf, G.R., Vautard, R., Vestreng, V., Vlachokostas, Ch., von Glasow, R., 2009. Atmospheric composition change – global and regional air quality. Atmos. Environ. 43, 5268–5350. https://doi.org/10.1016/j.atmosenv.2009.08.021.

Mudarra, M., Andreo, B., 2010. Hydrogeological functioning of a karst aquifer deduced from hydrochemical components and natural organic tracers present in spring waters. The case of Yedra spring (southern Spain). Acta Carsologica 39. https://doi.org/10.3986/ac.v39i2.98.

Mujalli Romero, G., 2019. The Role of Temperature in Processes Controlling Weathering Rates of Carbonate Lithologies and Volcanic Systems.

Nicholson, R. v, Gillham, R.W., Reardon, E.J., 1988. Pyrite oxidation in carbonate-buffered solution: 1. Experimental kinetics. Geochim. Cosmochim. Acta 52, 1077–1085. https://doi.org/10.1016/0016-7037(88)90262-1.

Pascaud, A., Sauvage, S., Coddeville, P., Nicolas, M., Croisé, L., Mezdour, A., Probst, A., 2016a. Contrasted spatial and long-term trends in precipitation chemistry and deposition fluxes at rural stations in France. Atmos. Environ. 146, 28–43. https://doi.org/10.1016/j.atmosenv.2016.05.019.

Pascaud, A., Sauvage, S., Pagé, C., Roustant, O., Probst, A., Nicolas, M., Croisé, L., Mezdour, A., Coddeville, P., 2016b. Composition chimique des dépôts atmosphériques à l'horizon 2020-2040. La Météorologie 8, 56. https://doi.org/10.4267/2042/58223.

Perrin, A.S., Probst, A., Probst, J.-L., 2008. Impact of nitrogenous fertilizers on carbonate dissolution in small agricultural catchments: implications for weathering CO2 uptake at regional and global scales. Geochim. Cosmochim. Acta 72, 3105–3123. https://doi.org/10.1016/j.gca.2008.04.011.

Pierret, M.C., Viville, D., Dambrine, E., Cotel, S., Probst, A., 2019. Twenty-five year record of chemicals in open field precipitation and throughfall from a medium-altitude forest catchment (Strengbach - NE France): an obvious response to atmospheric pollution trends. Atmos. Environ. 202, 296–314. https://doi.org/10.1016/j.atmosenv.2018.12.026.

Pointereau, P., Coulon, F., 2009. Abandon et artificialisation des terres agricoles. Le Courrier de l'environnement de l'INRA 57, 109–120.

Ponnou-Delaffon, V., Probst, A., Payre-Suc, V., Granouillac, F., Ferrant, S., Perrin, A.-S., Probst, J.-L., 2020. Long and short-term trends of stream hydrochemistry and high frequency surveys as indicators of the influence of climate change, agricultural practices and internal processes (Aurade agricultural catchment, SW France). Ecol. Indic. 110, 105894. https://doi.org/10.1016/J.ECOLIND.2019.105894.

Probst, A., Ambroise, B., 2019. Disturbance and resilience of a granitic critical zone submitted to acid atmospheric influence (the Ringelbach catchment, Vosges Mountains, France): lessons from a hydrogeochemical survey in the nineties. J. Hydrol. (Amst) 569, 77–92. https://doi.org/10.1016/J.JHYDROL.2018.11.018.

Probst, A., Fritz, B., Viville, D., 1995. Mid-term trends in acid precipitation, streamwater chemistry and element budgets in the strengbach catchment (Vosges Mountains, France). Water Air Soil Pollut. 79, 39–59. https://doi.org/10.1007/BF01100429.

Probst, J.L., 1983. Hydrologie du bassin de la Garonne. Modèle de mélanges. Bilan de l'érosion. Exportation des phosphates et des nitrates (PhD thesis).. University Paul Sabatier, Toulouse.

Probst, J.-L., Bazerbachi, A., 1986. Transports en solution et en suspension par la Garonne supérieure. Solute and particulate transports by the upstream part of the Garonne river. Sci. Géol. Bull. 39, 79–98. https://doi.org/10.3406/sgeol.1986.1720.

Probst, J.L., Tardy, Y., 1985. Fluctuations hydroclimatiques du Bassin d ' Aquitaine au cours des 70 dernieres annees. Rev. Géol. Dynam. Géog. Phys. 26, 59–76.

Qin, C., Li, S.-L., Waldron, S., Yue, F.-J., Wang, Z.-J., Zhong, J., Ding, H., Liu, C.-Q., 2020. High-frequency monitoring reveals how hydrochemistry and dissolved carbon respond to rainstorms at a karstic critical zone, southwestern China. Sci. Total Environ. 714, 136833. https://doi.org/10.1016/J.SCITOTENV.2020.136833.

Rabbinge, R., van Diepen, C.A., 2000. Changes in agriculture and land use in Europe. Eur. J. Agron. 13, 85–99. https://doi.org/10.1016/S1161-0301(00)00067-8.

Ran, L., Lu, X.X., Richey, J.E., Sun, H., Han, J., Yu, R., Liao, S., Yi, Q., 2015. Long-term spatial and temporal variation of CO_2 partial pressure in the Yellow River, China. Biogeosciences 12, 921–932. https://doi.org/10.5194/bg-12-921-2015.

Raymond, P.A., Oh, N.-H., Turner, R.E., Broussard, W., 2008. Anthropogenically enhanced fluxes of water and carbon from the Mississippi River. Nature 451, 449.

Reed, M.S., Bonn, A., Slee, W., Beharry-Borg, N., Birch, J., Brown, I., Burt, T.P., Chapman, D., Chapman, P.J., Clay, G.D., Cornell, S.J., Fraser, E.D.G., Glass, J.H., Holden, J., Hodgson, J.A., Hubacek, K., Irvine, B., Jin, N., Kirkby, M.J., Kunin, W.E., Moore, O., Moseley, D., Prell, C., Price, M.F., Quinn, C.H., Redpath, S., Reid, C., Stagl, S., Stringer, L.C., Termansen, M., Thorp, S., Towers, W., Worrall, F., 2009. The

future of the uplands. Land Use Policy 26, S204–S216. https://doi.org/10.1016/j.landusepol.2009.09.013.
Regnier, P., Resplandy, L., Najjar, R.G., Ciais, P., 2022. The land-to-ocean loops of the global carbon cycle. Nature. https://doi.org/10.1038/s41586-021-04339-9.
Rocher-Ros, G., Sponseller, R.A., Lidberg, W., Mörth, C.M., Giesler, R., 2019. Landscape process domains drive patterns of CO2 evasion from river networks. Limnol. Oceanogr. Lett. https://doi.org/10.1002/lol2.10108.
Romero-Mujalli, G., Hartmann, J., Börker, J., Gaillardet, J., Calmels, D., 2018. Ecosystem controlled soil-rock pCO2 and carbonate weathering – constraints by temperature and soil water content. Ann. N. Y. Acad. Sci. 769, 71–84. https://doi.org/10.1016/j.chemgeo.2018.01.030.
Roy, S., Négrel, P., 2001. A Pb isotope and trace element study of rainwater from the massif central (France). Sci. Total Environ. 277, 225–239. https://doi.org/10.1016/S0048-9697(00)00883-4.
Schulte, P., van Geldern, R., Freitag, H., Karim, A., Négrel, P., Petelet-Giraud, E., Probst, A., Probst, J.-L., Telmer, K., Veizer, J., Barth, J.A.C., 2011. Applications of stable water and carbon isotopes in watershed research: weathering, carbon cycling, and water balances. Earth Sci. Rev. 109, 20–31. https://doi.org/10.1016/j.earscirev.2011.07.003.
Semhi, K., Clauer, N., Probst, J.L., 2000. Strontium isotope compositions of river waters as records of lithology-dependent mass transfers: the Garonne river and its tributaries (SW France). Chem. Geol. 168, 173–193. https://doi.org/10.1016/S0009-2541(00)00226-6.
Sheng, H., Yang, Y., Yang, Z., Chen, G., Xie, J., Guo, J., Zou, S., 2010. The dynamic response of soil respiration to land-use changes in subtropical China. Glob. Chang. Biol. 16, 1107–1121. https://doi.org/10.1111/j.1365-2486.2009.01988.x.
Sivelle, V., Labat, D., Mazzilli, N., Massei, N., Jourde, H., 2019. Dynamics of the flow exchanges between matrix and conduits in karstified watersheds at multiple temporal scales. Water 11 (3), 569. https://doi.org/10.3390/w11030569.
Stanley, E.H., Loken, L.C., Casson, N.J., Oliver, S.K., Sponseller, R.A., Wallin, M.B., Zhang, L., Rocher-Ros, G., 2023. GRiMeDB: the Global River methane database of concentrations and fluxes. Earth Syst. Sci. Data 15, 2879–2926. https://doi.org/10.5194/essd-15-2879-2023.
Stets, E.G., Kelly, V.J., Crawford, C.G., 2014. Long-term trends in alkalinity in large rivers of the conterminous US in relation to acidification, agriculture, and hydrologic modification. Sci. Total Environ. 488–489, 280–289. https://doi.org/10.1016/J.SCITOTENV.2014.04.054.
Stockmann, U., Adams, M.A., Crawford, J.W., Field, D.J., Henakaarchchi, N., Jenkins, M., Minasny, B., McBratney, A.B., Courcelles, V. de R. de, Singh, K., Wheeler, I., Abbott, L., Angers, D.A., Baldock, J., Bird, M., Brookes, P.C., Chenu, C., Jastrow, J. D., Lal, R., Lehmann, J., O'Donnell, A.G., Parton, W.J., Whitehead, D., Zimmermann, M., 2013. The knowns, known unknowns and unknowns of sequestration of soil organic carbon. Agric. Ecosyst. Environ. 164, 80–99. doi:https://doi.org/10.1016/j.agee.2012.10.001.
Sytiuk, A., Cereghino, R., Hamard, S., Delarue, F.F., Dorrepaal, E., Kuttim, M., Lamentowicz, M., Pourrut, B., Robroek, B.J.M., Tuittila, E.-S., Jassey, V.E.J., Céréghino, R., Hamard, S., Delarue, F.F., Dorrepaal, E., Lamentowicz, M., Pourrut, B., Robroek, B.J.M., Tuittila, E.-S., Jassey, V.E.J., 2020. Morphological and biochemical responses of Sphagnum mosses to environmental changes. bioRxiv 2020, 10.29.360388.
Szczypta, C., Gascoin, S., Houet, T., Hagolle, O., Dejoux, J.F., Vigneau, C., Fanise, P., 2015. Impact of climate and land cover changes on snow cover in a small Pyrenean catchment. J. Hydrol. (Amst) 521, 84–99. https://doi.org/10.1016/j.jhydrol.2014.11.060.
Szramek, K., McIntosh, J.C., Williams, E.L., Kanduc, T., Ogrinc, N., Walter, L.M., 2007. Relative weathering intensity of calcite versus dolomite in carbonate-bearing temperate zone watersheds: carbonate geochemistry and fluxes from catchments within the St. Lawrence and Danube river basins. Geochem. Geophys. Geosyst. 8. https://doi.org/10.1029/2006GC001337.
Ulloa-Cedamanos, F., Probst, J.L., Binet, S., Camboulive, T., Payre-Suc, V., Pautot, C., Bakalowicz, M., Beranger, S., Probst, A., 2020. A forty-year karstic critical zone survey (baget catchment, pyrenees-France): lithologic and hydroclimatic controls on seasonal and inter- annual variations of stream water chemical composition, pCO2, and carbonate equilibrium. Water (Basel) 12, 1227. https://doi.org/10.3390/W12051227.
Ulloa-Cedamanos, F., Probst, A., Dos-Santos, V., Camboulive, T., Granouillac, F., Probst, J.-L., 2021a. Stream hydrochemical response to flood events in a multi-lithological karstic catchment from the Pyrenees Mountains (SW France). Water (Basel) 13, 1818.
Ulloa-Cedamanos, F., Probst, A., Moussa, I., Probst, J.-L., 2021b. Chemical weathering and CO2 consumption in a multi-lithological karstic critical zone: long term hydrochemical trends and isotopic survey. Chem. Geol. 585, 120567. https://doi.org/10.1016/j.chemgeo.2021.120567.
Ulloa-Cedamanos, F., Probst, J.L., Marais-Sicre, C., Vrech, E., Maire, E., Probst, A., 2022. Potential influence of landscape transition on stream water chemistry trends during the last decades in a karst catchment (Pyrenees, SW France) in a context of global environmental changes. Ecol. Indic. 140. https://doi.org/10.1016/j.ecolind.2022.109023.
Wallin, M.B., Campeau, A., Audet, J., Bastviken, D., Bishop, K., Kokic, J., Laudon, H., Lundin, E., Löfgren, S., Natchimuthu, S., Sobek, S., Teutschbein, C., Weyhenmeyer, G.A., Grabs, T., 2018. Carbon dioxide and methane emissions of Swedish low-order streams—a national estimate and lessons learnt from more than a decade of observations. Limnol. Oceanogr. Lett. 3, 156–167. https://doi.org/10.1002/lol2.10061.
Winkler, K., Fuchs, R., Rounsevell, M., Herold, M., 2021. Global land use changes are four times greater than previously estimated. Nat. Commun. 12, 2501. https://doi.org/10.1038/s41467-021-22702-2.
Wiśniewski, P., Märker, M., 2021. Comparison of topsoil organic carbon stocks on slopes under soil-protecting forests in relation to the adjacent agricultural slopes. Forests 12. https://doi.org/10.3390/f12040390.
Xiong, L., Bai, X., Zhao, C., Li, Y., Tan, Q., Luo, G., Wu, L., Chen, F., Li, C., Ran, C., Xi, H., Luo, X., Chen, H., Zhang, S., Liu, M., Gong, S., Xiao, B., Du, C., Song, F., 2022. High-resolution data sets for global carbonate and silicate rock weathering carbon sinks and their change trends. Earths. Future 10, e2022EF002746. https://doi.org/10.1029/2022EF002746.
Yuanrong, S., Ruihong, Y., Mingyang, T., Xiankun, Y., Lishan, R., Haizhu, H., Zhuangzhuang, Z., Xixi, L., 2021. Major ion chemistry in the headwater region of the Yellow River: impact of land covers. Environ. Earth Sci. 80, 398. https://doi.org/10.1007/s12665-021-09692-6.
Yue, F.J., Waldron, S., Li, S.L., Wang, Z.J., Zeng, J., Xu, S., Zhang, Z.C., Oliver, D.M., 2019. Land use interacts with changes in catchment hydrology to generate chronic nitrate pollution in karst waters and strong seasonality in excess nitrate export. Sci. Total Environ. 696, 134062. https://doi.org/10.1016/j.scitotenv.2019.134062.
Zeng, C., Liu, Z., Zhao, M., Yang, R., 2016. Hydrologically-driven variations in the karst-related carbon sink fluxes: insights from high-resolution monitoring of three karst catchments in Southwest China. J. Hydrol. (Amst) 533, 74–90. https://doi.org/10.1016/j.jhydrol.2015.11.049.
Zeng, Q., Liu, Z., Chen, B., Hu, Y., Zeng, S., Zeng, C., Yang, R., He, H., Zhu, H., Cai, X., Chen, J., Ou, Y., 2017. Carbonate weathering-related carbon sink fluxes under different land uses: a case study from the Shawan simulation test site, Puding, Southwest China. Chem. Geol. 474, 58–71. https://doi.org/10.1016/j.chemgeo.2017.10.023.
Zeng, S., Liu, Z., Kaufmann, G., 2019. Sensitivity of the global carbonate weathering carbon-sink flux to climate and land-use changes. Nat. Commun. 10. https://doi.org/10.1038/s41467-019-13772-4.
Zeng, S., Liu, Z., Goldscheider, N., Frank, S., Goeppert, N., Kaufmann, G., Zeng, C., Zeng, Q., Sun, H., 2021. Comparisons on the effects of temperature, runoff, and land-cover on carbonate weathering in different karst catchments: insights into the future global carbon cycle. Hydrogeol. J. 29, 331–345. https://doi.org/10.1007/s10040-020-02252-5.